JBC RESEARCH ARTICLE

An evolutionarily conserved N-terminal leucine is essential for MX1 GTPase antiviral activity against different families of RNA viruses

Received for publication, May 3, 2022, and in revised form, November 14, 2022 Published, Papers in Press, November 25, 2022,
https://doi.org/10.1016/j.jbc.2022.102747

Joe McKellar, Mary Arnaud-Arnould, Laurent Chaloin, Marine Tauziet, Charlotte Arpin-André, Oriane Pourcelot, Mickaël Blaise, Olivier Moncorgé*, and Caroline Goujon*

From the IRIM, CNRS, Montpellier University, Montpellier, France

Edited by Craig Cameron

Myxovirus resistance protein 1 (MX1) and MX2 are homologous, dynamin-like large GTPases, induced upon interferon exposure. Human MX1 (HsMX1) is known to inhibit many viruses, including influenza A virus, by likely acting at various steps of their life cycles. Despite decades of studies, the mechanism(s) of action with which MX1 proteins manage to inhibit target viruses is not fully understood. MX1 proteins are mechano-enzymes and share a similar organization to dynamin, with a GTPase domain and a carboxy-terminal stalk domain, connected by a bundle signaling element. These three elements are known to be essential for antiviral activity. HsMX1 has two unstructured regions, the L4 loop, also essential for antiviral activity, and a short amino (N)-terminal region, which greatly varies between MX1 proteins of different species. The role of this N-terminal domain in antiviral activity is not known. Herein, using mutagenesis, imaging, and biochemical approaches, we demonstrate that the N-terminal domain of HsMX1 is essential for antiviral activity against influenza A virus, Vesicular Stomatitis Virus, and La Crosse virus. Furthermore, we pinpoint a highly conserved leucine within this region, which is absolutely crucial for human, mouse, and bat MX1 protein antiviral activity. Importantly, mutation of this leucine does not compromise GTPase activity or oligomerization capabilities but does modify MX1 protein subcellular localization. The discovery of this essential and highly conserved residue defines this region as key for antiviral activity and may reveal insights as to the mechanism(s) of action of MX1 proteins.

Influenza A virus (IAV) is a member of the Orthomyxoviridae family and the causative agent of the disease commonly known as the flu. Upon infection of target epithelial cells within the respiratory tract, IAV is sensed by pattern recognition receptors, including retinoic acid-inducible gene I, which induce a signaling cascade leading to the production and secretion of type 1 and type 3 interferons (IFNs). The IFNs act in a paracrine and autocrine manner and, through binding to their cognate receptors and activation of the Janus Kinase/Signal transducer and activator of transcription pathway, leads to the regulation of hundreds of IFN-stimulated genes. Among these IFN-stimulated genes, many antiviral restriction factors have been described (1). These factors establish a so-called antiviral state, powerfully limiting IAV replication (2). The study of the IFN response against IAV in mice led to the discovery of the Myxovirus resistance (MX) proteins, which were later identified in humans (3–6). There are two homologous MX genes in humans, *MX1* and *MX2*. Human MX1, also called MxA (and hereafter referred to as HsMX1), inhibits a wide range of RNA and DNA viruses, replicating either in the cytoplasm, such as bunyavirus La Crosse Virus (LACV) and rhabdovirus Vesicular Stomatitis Virus (VSV), or in the nucleus, such as IAV (7). Human MX2 (HsMX2), or MxB, has notably been shown to potently inhibit HIV-1 and Herpes viruses (8–13). Interestingly, mice also possess two Mx proteins: MmMx1 and MmMx2. The latter is more closely related to HsMX1 than the former, but interestingly, MmMx1 is a more potent inhibitor of IAV than HsMX1 (14). However, to our knowledge, MmMx1 only restricts orthomyxoviruses, whereas HsMX1 is broadly antiviral and MmMx2 inhibits VSV and Hantaan River Virus (HTNV) (7). This difference could be due partly to the fact that MmMx1 is mainly localized inside the nucleus (15, 16), contrary to HsMX1 which is cytosolic.

Dynamin-like GTPases all share a very similar general organization and members of this family of proteins can present almost superimposable 3D crystal structures (17, 18). The 3D structure of HsMX1 has been partially solved (19, 20) (Fig. 1*A*). HsMX1 sports a globular head, which contains the GTPase module, and possesses a stalk domain, attached to the head by a tripartite bundle signaling element (BSE), composed of three separate alpha-helices (α-helices) that allow the fold-back of the stalk towards the GTPase domain, which is akin to dynamin (21) (Fig. 1*A*). The major difference between HsMX1 and dynamin is the lack in the former of the Pleckstrin Homology domain, essential for the PI(4,5)P2 binding capacity of dynamin (22). In place of the Pleckstrin Homology domain, HsMX1 has a flexible loop, termed loop L4, of which the structure is unresolved (Fig. 1*A*). Another unstructured loop, the L2 loop, is also found at the extremity of the stalk and in the vicinity of

* For correspondence: Olivier Moncorgé, olivier.moncorge@irim.cnrs.fr; Caroline Goujon, caroline.goujon@irim.cnrs.fr.

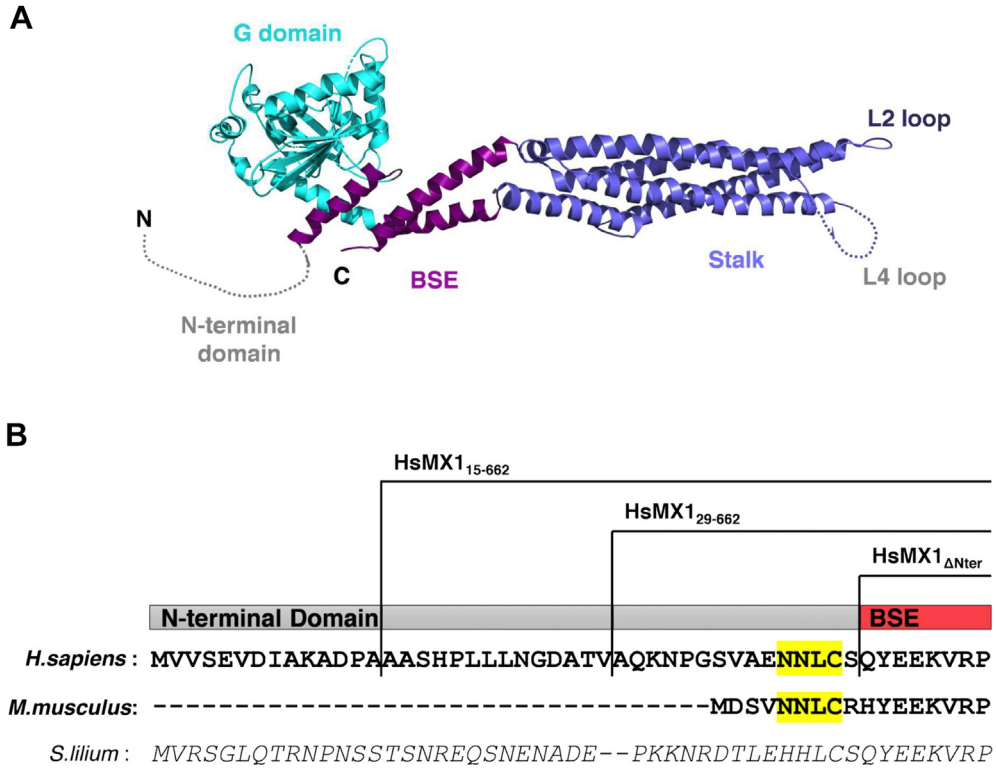

Figure 1. Tridimensional structure of HsMX1 and alignments of MX1 protein N-terminal domains. *A*, crystal structure of HsMX1 from (20); PDB: 3SZR. The N-terminal domain and L4 loop (randomly oriented *gray dotted lines*) have unknown structures. *B*, alignment of N-terminal domains of MX1 proteins of *Homo sapiens* (Human; P20591), *Mus musculus* (Mouse; Q3UD61), and *Sturnira lilium* (little *yellow*-shouldered bat; A0A1N7THZ1). HsMX1 N-terminal domain truncation mutations are represented and the NNLC motif is highlighted in *yellow*.

the L4 loop (Fig. 1*A*). In addition to these domains, HsMX1 and all MX proteins possess an amino-terminal (N-terminal) extension of unknown structure, which highly varies in length and sequence (Figs. 1, *A*, *B* and S1). HsMX1 has been shown to homodimerize through the stalk domain and further oligomerizes through numerous other interfaces on the stalk and the GTPase domains (19, 20, 23, 24). This may suggest the possible cohabitation of different types of HsMX1 oligomers within the cell. Of note, MmMx1 possesses a nuclear localization signal localized in the third α-helix of the BSE (25) allowing transport into the nucleus as opposed to HsMX1 and MmMx2, which are uniquely cytoplasmic.

The detailed antiviral mechanism(s) of action of MX1 proteins remain largely misunderstood, although certain intrinsic antiviral determinants have been well characterized. Four essential determinants have been identified to this day, the first being the binding/hydrolysis of GTP by the GTPase domain (26). Interestingly, HsMX2 does not require a functional GTPase domain for HIV-1 inhibition (8, 9, 27) and in the case of HsMX1, this might also be true for Hepatitis B Virus inhibition (28). The second determinant is the presence of an intact BSE (29), the third being the possibility to oligomerize *via* the stalk domain (19), and the fourth requirement involves the extremity of the stalk, loops L2 (30–32) and L4 (33–35). Indeed, deletions or point mutations of the L4 loop of HsMX1 and MmMx1 abrogated antiviral activity against IAV and Thogoto virus (33–35) and this loop was elegantly shown to have been under positive selection during evolution (36). Taken together, these studies showed that a number of intrinsic elements are needed for MX1 protein antiviral activity; however, to our knowledge, no study has so far addressed in depth the importance of the N-terminal domain of MX1 proteins. The N-terminal domain of HsMX2, however, which is longer than that of HsMX1 (91 amino acids compared to 43 amino acids) has been shown to be a crucial determinant for HIV-1 restriction (27, 37, 38). Transferring the N-terminal domain of HsMX2 onto HsMX1 resulted in a chimeric protein able to inhibit HIV-1, without losing the anti-IAV activity (27). These data prompt that the N-terminal domain of MX proteins may generally be important for antiviral activity.

In this study, we examined the role of the N-terminal domain of several MX1 proteins, showing that this domain is essential for antiviral activity. Indeed, deletion of the N-terminal region abrogates antiviral activity against IAV and this effect was mapped to a single essential residue, leucine 41 (L41) in HsMX1. This residue was also essential for the inhibition of rhabdoviruses and bunyaviruses. We further show that this residue is highly conserved between MX1 proteins of different origins, and we show that the corresponding leucines in MmMx1 (leucine 7, L7) and little yellow-shouldered bat, *Sturnira lilium* MX1 (SlMX1) (leucine 39, L39) are also essential for anti-IAV activity. Finally, we demonstrate that mutation of this highly conserved leucine did not seem to impact lower- or higher-order oligomerization status of HsMX1 or MmMx1 in cells, the propensity to hydrolyze GTP *in vitro*, or the natural structure of the first BSE α-helix *in*

silico. However, we show that this residue is essential for correct subcellular localization of MX1 proteins. This study therefore confirms the complex multimodular nature of MX1 proteins and defines their N-terminal region as another important antiviral module governed by an essential and highly conserved leucine.

Results

Leucine 41 from the N-terminal region of human MX1 is essential for antiviral activity against IAV

The loop L4 and all 43 amino acids of the N-terminal domain are absent from the published crystal structures of HsMX1 (19, 20) (Fig. 1*A*). While the L4 loop has been extensively studied in the past (34, 36), to date, the importance of the N-terminal region for the antiviral activity of HsMX1 has not been evaluated. Therefore, to address this, we generated a series of N-terminal truncation mutants for HsMX1, with mutants missing either the first 14 ($HsMX1_{15\text{-}662}$) or 28 ($HsMX1_{29\text{-}662}$) amino acids or the entire N-terminal region ($HsMX1_{44\text{-}662}$, named hereafter $HsMX1_{\Delta Nter}$) (Fig. 1*B*). In parallel to two negative controls (E2-Crimson fluorescent protein, termed CTRL, and HsMX1 inactive GTPase mutant, $HsMX1_{T103A}$), the WT protein and mutants were ectopically expressed in Human Embryonic Kidney 293T (HEK293T) cells and an IAV minigenome infection reporter assay was performed, as reported previously (8). In this assay, a negative sense minigenome coding for the Firefly luciferase is recognized, replicated, and transcribed by IAV polymerase in IAV-infected cells. Thus, Firefly activity is used to monitor replication efficiency. Cells were also cotransfected with a Renilla luciferase coding plasmid for normalization. We observed that the deletion of the first 14 or 28 amino acids had no effect on HsMX1 antiviral activity (Fig. 2*A* top panel). In contrast, the deletion of the entire N-terminal region totally abrogated antiviral activity in a comparable manner to the control-inactive GTPase mutant $HsMX1_{T103A}$ (Fig. 2*A* top panel). This suggested the presence of essential residues located between positions 29 and 43 of the N-terminal domain of HsMX1. *Mus musculus* Mx1 (MmMx1) is another well-studied IAV-inhibiting MX1 protein. Alignment of MmMx1 and HsMX1 proteins revealed a conserved motif of four amino acids located between positions 29 and 43 of HsMX1: 39-NNLC-42 (or 5-NNLC-8 in the case of MmMx1) (Fig. 1*B*). Upon replacement in HsMX1 of these four amino acids with four alanines ($HsMX1_{NNLC39\text{-}42A}$), we saw a complete loss of antiviral activity comparable to that of $HsMX1_{\Delta Nter}$ and $HsMX1_{T103A}$ (Fig. 2*A*, top panel). Alanine point mutations of these four residues ($HsMX1_{N39A}$, $HsMX1_{N40A}$, $HsMX1_{L41A}$, and $HsMX1_{C42A}$) revealed that leucine 41 (L41) was responsible for the loss-of-function phenotype observed with the $MX1_{NNLC39\text{-}42A}$ mutant, whereas the other three mutants completely retained their anti-IAV activity (Fig. 2*A*, top panel). While the $HsMX1_{29\text{-}662}$ and $HsMX1_{\Delta Nter}$ truncation mutants showed decreased expression levels compared to the WT protein, as assessed by immunoblotting, the loss of antiviral activity of the $HsMX1_{NNLC39\text{-}42A}$ and $HsMX1_{L41A}$ mutants could not be attributed to a decrease in expression levels (Fig. 2*A*, bottom panel).

The observed phenotypes were then confirmed using a Nanoluciferase reporter–expressing version of A/Victoria/3/75 (IAV-NLuc) (39) as a second infection readout, both in HEK293T (Fig. 2*B*) and in lung-derived A549 cells (Fig. 2*C*), which stably expressed the control and mutant proteins. Similarly to what was observed in the minigenome infection reporter assay (Fig. 2*A*), $HsMX1_{\Delta Nter}$, $HsMX1_{NNLC39\text{-}42A}$, and $HsMX1_{L41A}$ were completely inactive against IAV, comparable to the inactive $HsMX1_{T103A}$ mutant, whereas the other mutants retained antiviral activity (Fig. 2, *B* and *C*). Finally, to confirm that the $HsMX1_{L41A}$ mutant also showed a loss of antiviral activity in multiround infection experiments, we performed A/Victoria/3/75 WT virus growth curves in A549 cells stably expressing either HsMX1, the inactive $HsMX1_{T103A}$ mutant as a negative control, or $HsMX1_{L41A}$. HsMX1 inhibited IAV replication by around two logs compared to the $HsMX1_{T103A}$ control at all time points (Fig. 2*D*). The $HsMX1_{L41A}$ mutant showed comparable virus yields to $HsMX1_{T103A}$, confirming the inability of this mutant to inhibit IAV replication (Fig. 2*D*).

Next, we investigated the subcellular localization of the N-terminal HsMX1 mutants using super-resolution Airyscan microscopy. As reported previously, HsMX1 showed a honeycomb-like, punctate cytoplasmic staining and $HsMX1_{T103A}$ presented a juxtanuclear accumulation (Fig. 2*E*) (24, 27, 40). In contrast, the $HsMX1_{\Delta Nter}$ mutant formed cytoplasmic aggregate-like structures that varied in size and were dispersed throughout the cytoplasm (Fig. 2*E*). Unlike this mutant, $HsMX1_{NNLC39\text{-}42A}$ and $HsMX1_{L41A}$ accumulated at the perinuclear region into small spherical structures that were phenotypically different from those of $HsMX1_{T103A}$ or $HsMX1_{\Delta Nter}$ (Fig. 2*E*). This attests to a potential difference between the L41 point and N-terminal truncation mutants, which might be linked to differences in protein synthesis or stability as seen by immunoblot (Fig. 2, *A*–*C*).

Taken together, these data showed that the N-terminal region, and more precisely, leucine 41, was essential for the anti-IAV activity and correct subcellular localization of HsMX1.

L41 is essential for HsMX1 restriction of other families of RNA viruses

To further understand the importance of this newly discovered essential residue for the antiviral activity of HsMX1, we tested the restriction abilities of aforementioned HsMX1 mutants against other RNA viruses known to be inhibited by HsMX1. HEK293T cells were cotransfected with either a control or HsMX1-WT or mutant expression constructs along with a Renilla luciferase–coding plasmid, and the infection levels of single-round rhabdovirus VSV firefly-expressing replicon particles (G-pseudotyped VSV*ΔG-fLuc particles (41)) were measured (Fig. 3*A*). Reminiscent of what was observed for IAV (Fig. 2*A*), the $HsMX1_{\Delta Nter}$, $HsMX1_{NNLC39\text{-}42A}$, and $HsMX1_{L41A}$ mutants totally lost their ability to restrict the VSV*ΔG-fLuc replicon (Fig. 3*A*). To

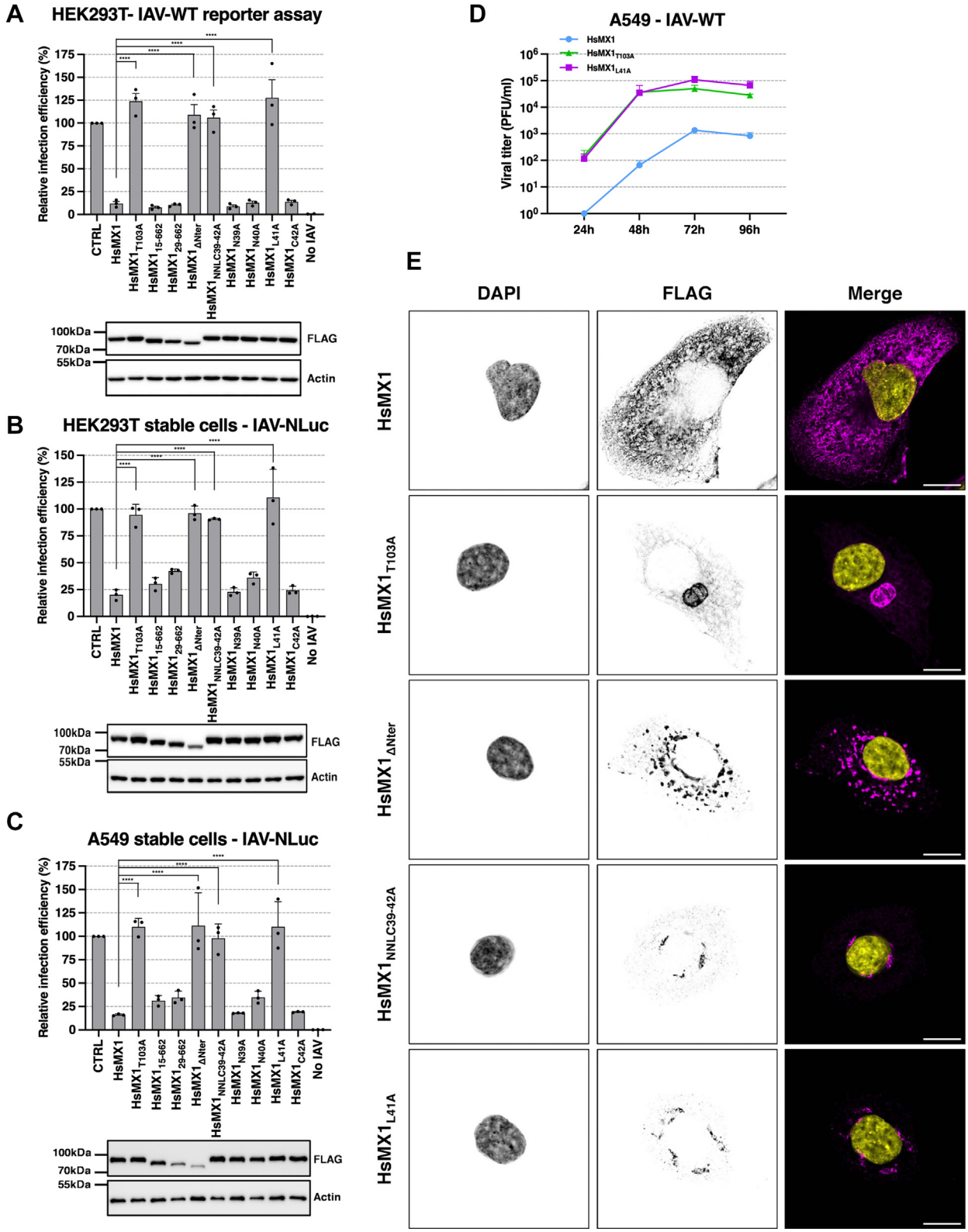

Figure 2. The N-terminal domain of HsMX1 is essential for IAV restriction and subcellular localization. *A*, relative infection efficiency using an influenza minigenome infection reporter assay in transiently transfected HEK293T cells with FLAG-tagged WT HsMX1, mutants, or E2-Crimson control (CTRL) (*top*), with a representative immunoblot (*bottom*; actin served as a loading control). *B*, relative infection efficiency of IAV-NLuc in HEK293T cells stably expressing FLAG-tagged proteins of interest (*top*), with a representative immunoblot (*bottom*; actin served as a loading control). *C*, relative infection efficiency of IAV-NLuc in A549 cells stably expressing the FLAG-tagged proteins of interest (*top*), with a representative immunoblot (*bottom*; actin served as a loading control). *D*, A549 cells stably expressing FLAG-tagged HsMX1, HsMX1$_{T103A}$, or HsMX1$_{L41A}$ were infected with A/Victoria/3/75 at MOI 0.005; the supernatants harvested at the indicated time points post infection and infectious virus production was measured by plaque assays on MDCK cells. Data shows one representative experiment with the mean and SDs of technical triplicates. *E*, representative Airyscan immunofluorescence images of A549 cells stably expressing the FLAG-tagged proteins of interest, stained for anti-FLAG (*magenta*) and nuclei (DAPI; *yellow*). Single channels are shown in inverted

confirm these results using WT VSV, BHK-21 cells stably expressing HsMX1, inactive $HsMX1_{T103A}$, or $HsMX1_{L41A}$ were infected at low multiplicity of infection (MOI, 0.01) for 24 h and viral production was measured by plaque assays on Vero cells. HsMX1 inhibited VSV replication by over one log compared to $HsMX1_{T103A}$, and $HsMX1_{L41A}$ did not impact viral replication, reaching similar titers as in the presence of $HsMX1_{T103A}$ (Fig. 3*B*). This therefore demonstrates the essential role of L41 for the restriction of VSV by HsMX1.

As HsMX1 is well known to inhibit the Orthobunyaviruses LACV and Bunyamwera Virus (BUNV) (42), we tested the importance of the N-terminal domain against these viruses. The inhibition phenotype of HsMX1 towards LACV and BUNV is characterized by the aggregation of their nucleoprotein into perinuclear aggregates (42), a phenotype that can be recapitulated by coexpressing HsMX1 and the nucleoprotein in cells and easily visualized by using a fusion of the LACV or BUNV nucleoprotein (LACV-N and BUNV-N) with the red fluorescent protein (RFP) (42). Hence, HEK293T cells were cotransfected with plasmids expressing HsMX1 or the mutants of interest, together with an RFP-LACV-N expression plasmid. As reported previously (42), HsMX1 induced LACV-N aggregation and this ability was lost by $HsMX1_{T103A}$, as shown on the representative images (Fig. 3*C*). To quantify HsMX1 protein activity here, the percentage of cells showing a diffuse or aggregated RFP-LACV-N staining was determined. In control conditions (RFP-LACV-N alone), around 70% of the cells displayed a diffuse cytoplasmic pattern (Fig. 3*D*), with 30% of cells showing limited aggregation, possibly due to overexpression levels. In the presence of HsMX1, only around 10% of cells showed a diffuse cytoplasmic staining, with around 90% of cells showing an RFP-LACV-N aggregation at the perinuclear region (Fig. 3, *D* and *C*). In the presence of $HsMX1_{\Delta Nter}$, $HsMX1_{NNLC39-42A}$, and $HsMX1_{L41A}$, there was a complete loss of RFP-LACV-N aggregation phenotype, with distributions comparable to the RFP-LACV-N alone or $HsMX1_{T103A}$ conditions (Fig. 3, *D* and *C*). The same experiment was performed for RFP-BUNV-N (Fig. 3*E*). Similar results to the ones obtained with LACV-N were observed, although with a somewhat reduced, but nevertheless significant, impact of $HsMX1_{NNLC39-42A}$ and $HsMX1_{L41A}$ mutations on the ability of HsMX1 to induce RFP-BUNV-N aggregation.

To confirm these results, we performed multiround infection experiments with LACV in BHK-21 cells that stably expressed HsMX1, inactive $HsMX1_{T103A}$, or $HsMX1_{L41A}$ (Fig. 3*F*). HsMX1 inhibited LACV replication by over one log at 48 and 72 h postinfection compared to $HsMX1_{T103A}$ and $HsMX1_{L41A}$, confirming that $HsMX1_{L41A}$ is not able to inhibit LACV replication.

These data show that the N-terminal domain, and in particular L41, is important for LACV and BUNV restriction as well as for VSV and IAV.

Importance of the N-terminal domain for the anti-IAV activity of MX1 proteins of other mammals

MX1 proteins from various mammalian species are known to harbor anti-IAV activity (7, 43). Therefore, we sought to explore the importance of the conserved leucine in the N-terminal region in the anti-IAV activity of MX1 proteins from other mammals. Mouse Mx1 (MmMx1) strongly inhibits IAV, and, interestingly, the N-terminal domain of MmMx1 is highly different to that of HsMX1, consisting of only nine amino acids *versus* 43 for HsMX1 (Fig. 1*B*). Nevertheless, MmMx1 contains a leucine at position 7, placed exactly three amino acids before the start of the first α-helix of the BSE domain, similarly to leucine 41 of HsMX1 (Fig. 1*B*). To determine whether the N-terminal domain, and notably L7, were also essential for MmMx1 anti-IAV activity, we performed a truncation of the N-terminal domain ($MmMx1_{\Delta Nter}$) and an alanine point mutation of L7 ($MmMx1_{L7A}$). We stably expressed these constructs, as well as the GTPase-inactive mutant ($MmMx1_{T69A}$), in A549 cells and infected them with the IAV-NLuc reporter virus (Fig. 4*A*, top panel). Whereas MmMx1 potently inhibited IAV replication, $MmMx1_{\Delta Nter}$ and $MmMx1_{L7A}$ showed no antiviral activity, similar to the GTPase inactive mutant $MmMx1_{T69A}$ (Fig. 4*A*, top panel). It is noteworthy that, similarly to $HsMX1_{\Delta Nter}$ (Fig. 2*A*), $MmMx1_{\Delta Nter}$ had reduced expression levels (Fig. 4*A*, bottom panel). However, $MmMx1_{L7A}$ showed similar expression levels as compared to WT MmMx1 (Fig. 4*A*, bottom panel). Using super-resolution Airyscan microscopy, WT MmMx1 was found to localize into classical MmMx1 nuclear bodies as well as being present to a lesser extent in the cytoplasm (Fig. 4*B*). $MmMx1_{T69A}$ was found as small irregularly localized nuclear bodies and also accumulated at the perinuclear region (Fig. 4*B*). $MmMx1_{\Delta Nter}$ formed nuclear rod-like structures, and $MmMx1_{L7A}$ was found as nuclear rod-like structures that associated into star-shaped superstructures, as well as in a perinuclear accumulation (Fig. 4*B*). Some cytoplasmic rod-like structures were also observed for this mutant (Fig. 4*B*). Of note, MmMx1 and $MmMx1_{L7A}$ seemed to displace the Hoechst staining locally (Fig. 4*B*). Taking all these data together, we show that the N-terminal domain, and more specifically leucine 7, is essential for MmMx1 anti-IAV activity and subcellular localization.

We then looked at a more distant relative of humans and chose to study a bat MX1 protein, *S. lilium* (little yellow-shouldered bat) MX1 (SlMX1), that also possesses anti-IAV activity (44). SlMX1 has a similar sized N-terminal domain (41 amino acids in length) to that of HsMX1, with again, a leucine located three amino acids before the start of the BSE, leucine 39 (L39) (Fig. 1*B*). As previously, we generated a truncation of the N-terminal domain ($SlMX1_{\Delta Nter}$) and an alanine point mutation of L39 ($SlMX1_{L39A}$). We produced A549 cells stably expressing WT and mutant SlMX1 and infected them with the IAV-NLuc reporter virus (Fig. 4*C*). As

gray; the scale bar represents 10 μm. The experiment was performed four times independently. (A-C) Results were normalized to 100% for the CTRL condition, and the mean and SDs of three independent experiments are shown. Ordinary one-way ANOVA multiple comparison with HsMX1 was performed; **** = $p < 0.0001$. HEK293T, Human Embryonic Kidney 293T; IAV, influenza A virus; MDCK, Madin-Darby canine kidney; PFU, plaque forming units.

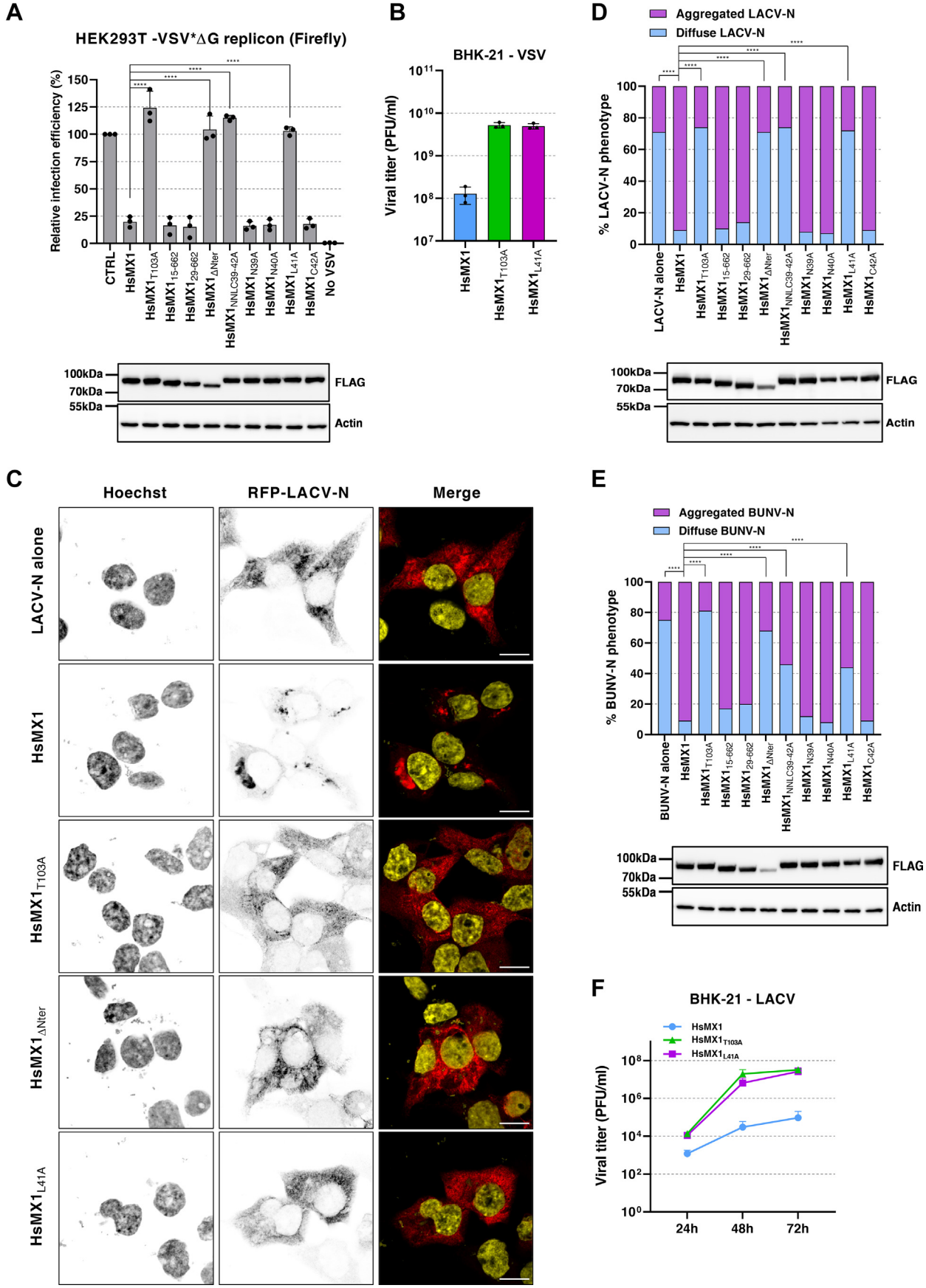

Figure 3. L41 is essential for restriction of other RNA viruses. *A*, relative VSV*ΔG-fLuc infection efficiency of HEK293T cells transfected with the indicated FLAG-tagged HsMX1 constructs or E2-Crimson (CTRL) (*top*), with a representative immunoblot (*bottom*; actin served as a loading control). *B*, BHK-21 cells

for HsMX1 and MmMx1, $SlMX1_{\Delta Nter}$ and $SlMX1_{L39A}$ mutants lost their antiviral activity against IAV, similar to the GTPase-inactive mutant $SlMX1_{T101A}$ (Fig. 4*C*, top panel). In opposition to $HsMX1_{\Delta Nter}$ and $MmMx1_{\Delta Nter}$, however, $SlMX1_{\Delta Nter}$ did not show profoundly decreased expression levels and the $SlMX1_{L39A}$ mutant seemed to show slightly higher expression levels than WT SlMX1 (Fig. 4*C*, bottom panel). In terms of subcellular localization, SlMX1 was found as cytoplasmic puncta forming honeycomb-like subcellular structures and the GTPase mutant $SlMX1_{T101A}$ showed a perinuclear accumulation phenotype, reminiscent of HsMX1 and $HsMX1_{T103A}$, respectively (Figs. 4*D* and 2*E*). In contrast, $SlMX1_{\Delta Nter}$ and $SlMX1_{L39A}$ were present in small puncta in the cytoplasm but lost their honeycomb-like network (Fig. 4*D*).

These data confirm that the conserved leucine present in the N-terminal domain of mammalian MX1 proteins is a crucial residue for their antiviral activity and subcellular localization.

The equivalent of L41 in HsMX1 is highly conserved across the animal kingdom

Considering that this leucine is conserved for human, mouse, and bat MX1 proteins, we aligned the amino acid sequence of MX1 proteins from 76 different animal species, comprising mammals, birds, amphibians, and fishes (Fig. S1). An analysis using the WebLogo3 tool (weblogo.threeplusone.com) (45, 46) of amino acids corresponding to positions 34-52 of HsMX1 from all 76 sequences of the alignment in Fig. S1 shows the extreme conservation of the leucine corresponding to L41 throughout all MX1 proteins aligned (Fig. 5*A*, an orange box defines position 41). Indeed, the leucine residue is conserved to a level similar to amino acids from the BSE domain (Fig. 5*A*). Of note, only a few species of fishes, including zebrafish (*Danio rerio*) and goldfish (*Carassius auratus*) did not show conservation of this leucine, with a phenylalanine (F) found instead (Fig. S1). To explore if this position could tolerate other amino acids, and to see if the naturally occurring phenylalanine replacement in some fish species led to a nonfunctional protein, we replaced L41 of HsMX1 with different types of amino acids. We chose aspartic acid (D) and lysine (K) as the representative of negative and positive charged side chains, respectively, asparagine (N) as the representative of the polar uncharged side chains, and proline (P) as an aliphatic nonpolar amino acid that can affect protein 3D structure. We also generated the $HsMX1_{L41F}$ mutant to mimic the naturally occurring phenylalanine at this position found in some fish species. Performing IAV minigenome infection reporter assays, we can see that replacing L41 with D, N, P, or K ($HsMX1_{L41D}$, $HsMX1_{L41N}$, $HsMX1_{L41P}$, and $HsMX1_{L41K}$) induced a total loss of antiviral activity against IAV, similar to the inactive mutants $HsMX1_{T103A}$ and $HsMX1_{L41A}$ (Fig. 5*B*). However, $HsMX1_{L41F}$ interestingly retained similar inhibition levels as the WT protein, suggesting that replacing leucine at this position with phenylalanine was tolerated and did not disturb antiviral activity (Fig. 5*B*). Of note, expression levels of all mutants were similar to that of the WT protein (Fig. 5*B* bottom panel).

These observations show the extreme conservation of the leucine residue for MX1 proteins of many different species and that the only natural variant identified remained functional, attesting to the importance of this residue for antiviral activity. This might further suggest that a strong evolutionary pressure has been exerted on this site.

Loss of antiviral activity of N-terminal leucine mutants is neither due to an oligomerization defect nor the inability to hydrolyze GTP

Correct oligomerization and GTPase activity being both essential for HsMX1 antiviral activity (19, 26), we wondered whether mutating L41 in HsMX1 could impair these properties. First, we performed crosslinking experiments on WT HsMX1, $HsMX1_{T103A}$, $HsMX1_{M527D}$ (a monomeric mutant (19)), and $HsMX1_{L41A}$. HEK293T cells stably expressing these proteins showed the expected phenotypes with respect to IAV-NLuc infection, with a loss of antiviral activity for $HsMX1_{M527D}$ comparable to that of $HsMX1_{T103A}$ and $HsMX1_{L41A}$ (Fig. 6*A*). Disuccinimidyl suberate crosslinking followed by immunoblotting experiments showed that, contrary to WT HsMX1, $HsMX1_{M527D}$ did not assemble into lower- or higher-order oligomers and was only detected as a monomer (Fig. 6*B*), as expected (19). In contrast, $HsMX1_{L41A}$ showed a similar capacity to oligomerize into lower- and higher-order oligomers than WT HsMX1 or the GTPase-inactive mutant $HsMX1_{T103A}$ (Fig. 6*B*). We can therefore conclude that the absence of antiviral activity of this mutant is not due to an oligomerization defect. As $HsMX1_{L41A}$ was able to multimerize, we next wondered whether it could have a dominant negative impact on WT HsMX1 similarly to $HsMX1_{T103A}$ (29). To explore this, we performed IAV minigenome infection reporter assays in cells cotransfected with Myc-tagged HsMX1 and increasing quantities of FLAG-tagged $HsMX1_{L41A}$ or $HsMX1_{T103A}$ (Fig. S2*A*). In contrast to $HsMX1_{T103A}$, which exerted a potent dominant negative effect on the antiviral activity of the WT protein, $HsMX1_{L41A}$

stably expressing FLAG-tagged HsMX1, $HsMX1_{T103A}$, or $HsMX1_{L41A}$ were infected in triplicates with VSV (MOI 0.01), and supernatants were collected 24 h postinfection for viral titration by plaque assays on Vero cells. *C*, representative Airyscan images of the phenotype of RFP-LACV-N in transfected HEK293T cells in the presence of different FLAG-tagged HsMX1 constructs. Single channels are shown in inverted *gray* and on the merge images, RFP-LACV-N is shown in *red*, and nuclei (Hoechst-33258) in *yellow*. The scale bar represents 10 μm. *D*, quantification of the percentage of RFP-LACV-N and WT or mutant FLAG-tagged HsMX1-transfected HEK293T cells presenting a diffuse or aggregated RFP-LACV-N staining (*top*), with a representative immunoblot (*bottom*; actin served as a loading control). *E*, similar to (*C*), with RFP-BUNV-N. *F*, BHK-21 cells stably expressing FLAG-tagged HsMX1, $HsMX1_{T103A}$, or $HsMX1_{L41A}$ were infected in triplicates with LACV at low MOI (0.005), and supernatants were collected at the indicated time points post infection for viral titration by plaque assays on Vero cells. The graphs show the mean and SDs of 3 (*A* and *D*), 2 (*E*), or 1 (*B* and *F*) independent replicates. A total of 1500 to 2000 cells (*D*) and 950 to 1250 cells (*E*) were counted for each condition, respectively. Ordinary one-way ANOVA multiple comparison with HsMX1 was performed. For (*D* and *E*), diffuse LACV-N or BUNV-N values were used; **** = $p < 0.0001$. HEK293T, Human Embryonic Kidney 293T; LACV, LaCrosse Virus; BUNV, Bunyamwera Virus; RFP, red fluorescent protein.

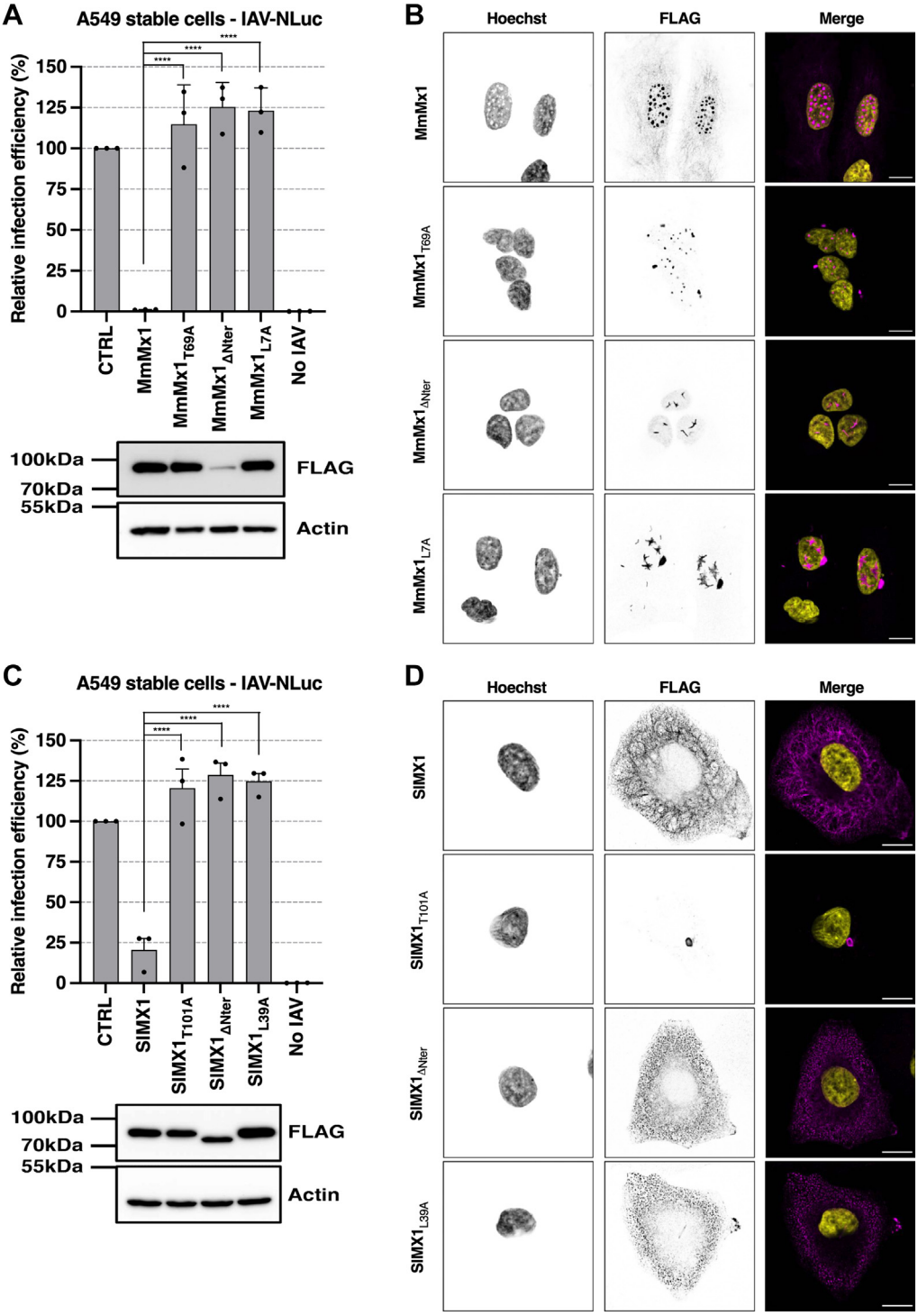

Figure 4. Importance of the N-terminal domains of MX1 proteins of other mammals. *A*, top panel, relative IAV-NLuc infection efficiency of A549 cells stably expressing FLAG-tagged E2-Crimson (CTRL), WT, or mutant MmMx1 proteins. *Bottom* panel, a representative immunoblot is shown. *B*, representative Airyscan images of A549 cells stably expressing FLAG-tagged MmMx1 or mutants. Single channels are shown in inverted *gray*, FLAG proteins in *magenta*, and nuclei (Hoechst-33258) in *yellow*; the scale bar represents 10 μm. *C*, *top panel*, relative IAV-NLuc infection efficiency of stable A549 cells stably expressing FLAG-tagged Renilla luciferase (CTRL), SIMX1, or mutants. *Bottom* panel, a representative immunoblot is shown. *D*, representative Airyscan images of A549 cells stably expressing FLAG-tagged SIMX1 or mutants (color code as in *B*); the scale bar represents 10 μm. For (*A* and *C*), the graphs show the mean and SD of three independent experiments. Ordinary one-way ANOVA multiple comparison with WT MmMx1 or SIMX1 was performed; **** = $p < 0.0001$. IAV, influenza A virus.

expression did not have a significant impact on HsMX1 antiviral activity. We then wondered whether WT HsMX1 and $HsMX1_{L41A}$ coexpression could have an effect on their respective subcellular localization patterns (Fig. S2*B*). We observed that Myc-tagged HsMX1 localization was similar to that of FLAG-HsMX1 (Fig. 2*E*) and was unmodified in the

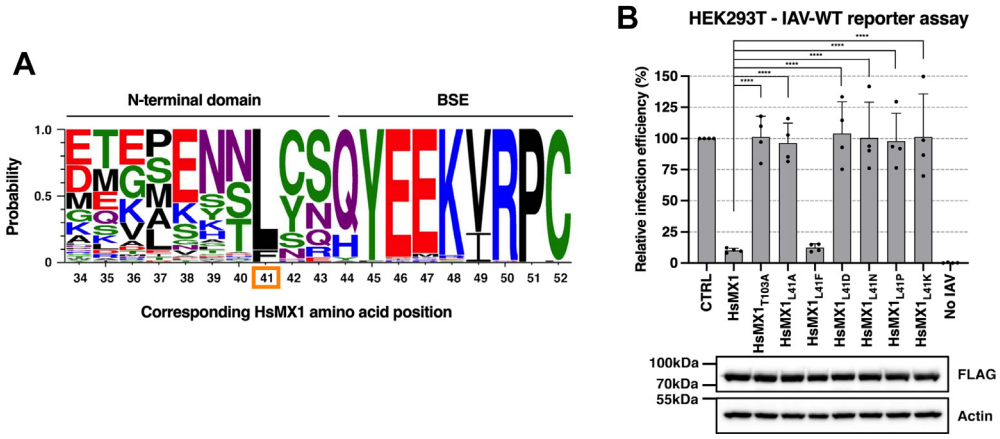

Figure 5. Evolutionary conservation of the leucine residue of MX1 proteins. *A*, WebLogo3 analysis of MX1 proteins from 76 different species. Amino acids of all protein sequences aligned correspond to those of HsMX1 numbering from position 34-52. Alignment was performed using the align tool from Uniprot (www.uniprot.org/align/). Full alignment can be found in Fig. S2. Colors represent amino acid chemistry groups. The position corresponding to HsMX1 L41 is indicated with an *orange box* around the residue number. *B*, relative infection efficiency using an influenza minigenome infection reporter assay in transiently transfected HEK293T cells with FLAG-tagged HsMX1, mutants, or E2-Crimson (CTRL) (*top*), with a representative immunoblot (*bottom*; actin served as a loading control). The mean and SD of four independent experiments are shown. Ordinary one-way ANOVA multiple comparison with WT HsMX1 was performed; **** = $p < 0.0001$. BSE, bundle signaling element; HEK293T, Human Embryonic Kidney 293T.

presence of FLAG-HsMX1$_{L41A}$ (Fig. S2*B*). In contrast, the localization of the latter was clearly impacted by the WT protein, as FLAG-HsMX1$_{L41A}$ could be found in the honeycomb-like network in cells expressing Myc-HsMX1 (Fig. S2*B*). Taken together, this suggested that HsMX1$_{L41A}$ might be able to associate with WT HsMX1 without significantly impeding its antiviral activity.

We next checked the ability of MmMx1 and mutants to multimerize in HEK293T cells to see if this protein acted similarly to HsMX1 in regards to the importance of the L7 for oligomerization (Fig. 6, *C* and *D*). Of note, MmMx1$_{M493D}$, the potential monomeric mutant corresponding to HsMX1$_{M527D}$, could not be used as its expression was undetectable (data not shown). MmMx1 stable overexpression in HEK293T cells strongly inhibited IAV replication, although somewhat less efficiently compared to stable overexpression in A549 cells (compare Fig. 6*C* with Fig. 4*A*). Both MmMx1$_{T69A}$ and MmMx1$_{L7A}$ mutants totally lost antiviral activity (Fig. 6*C*). In a similar fashion to HsMX1$_{L41A}$, MmMx1$_{L7A}$ was able to oligomerize into lower- and higher-order oligomers (Fig. 6*D*), showing that the inability of MmMx1$_{L7A}$ to inhibit IAV was not due to an oligomerization defect.

To assess the potential impact of leucine mutations on MX1 protein GTPase activity, recombinant WT HsMX1, MmMx1 and mutant proteins HsMX1$_{T103A}$, HsMX1$_{L41A}$, MmMx1$_{T69A}$, and MmMx1$_{L7A}$ were produced in *Escherichia coli* and purified (Fig. 7*A*). A GTPase activity assay was performed to assess the ability of these proteins to convert GTP into GDP (Fig. 7, *B* and *C*). While HsMX1 and the GTPase-inactive mutant HsMX1$_{T103A}$ were respectively able and unable to hydrolyze GTP, as expected (47) (Fig. 7*B*), the HsMX1$_{L41A}$ mutant showed comparable GTPase activity to WT HsMX1, indicating no defect in enzymatic activity. In the case of MmMx1, WT MmMx1 could hydrolyze GTP, and MmMx1$_{T69A}$ was unable to hydrolyze it (Fig. 7*C*), as expected (35). However, while MmMx1$_{L7A}$ was still able to hydrolyze GTP to some extent, in comparison to WT MmMx1, MmMx1$_{L7A}$ showed ∼60% decrease in enzymatic activity (Fig. 7*C*). Time course experiments showed that GTPase activity efficiency of HsMX1$_{L41A}$ was identical to that of WT HsMX1 regardless of the duration of the assay (Fig. 7*D*). In contrast, MmMx1$_{L7A}$ appeared less active than WT MmMx1 and showed a 30% to 50% decrease in GTPase activity at the different time points (Fig. 7*E*). Nevertheless, these experiments showed that the loss of antiviral activity of HsMX1$_{L41A}$ and MmMx1$_{L7A}$ mutants could not be attributed to a complete inability to hydrolyze GTP.

Mutating L41 of HsMX1 does not seem to impact BSE structural properties

As mentioned above, the structure of the N-terminal domain of HsMX1 has not been solved (19, 20) (Fig. 1*A*). The AlphaFold tool (48, 49) may accurately predict structures of proteins (or regions of proteins) that have not been experimentally determined by structural approaches. Concerning HsMX1, the N-terminal domain can be modeled starting from serine 35 (S35) (alphafold.ebi.ac.uk/entry/P20591), although the confidence levels are not high and even lower for the long N-terminal unstructured tail. Nevertheless, AlphaFold predicts that the first α-helix of the BSE starts at S35, which would entail a redefinition of BSE region and would make L41 actually part of the BSE (Fig. 8*A*). Hence, mutation of L41 into an alanine could cause a restructuration of the BSE helix, explaining the loss of antiviral activity of the HsMX1$_{L41A}$ mutant. However, performing molecular dynamics (MD) simulations with WT HsMX1 or the L41A mutant (Fig. 8, *B* and *C*, Movies S1 and S2) showed that the structural behavior of this α-helix did not change when comparing both proteins. Indeed, except for a hinge or a turn-like structure occurring quite rapidly around residues E46-E47 but observed in both cases, the α-helicoidal secondary structure is maintained all throughout the simulations (0.5 μs) (Fig. 8, *B* and *C*, Movies S1 and S2). To confirm this point, two dihedral angles (Phi and Psi) from part of the N-terminal helix (residues ranging from

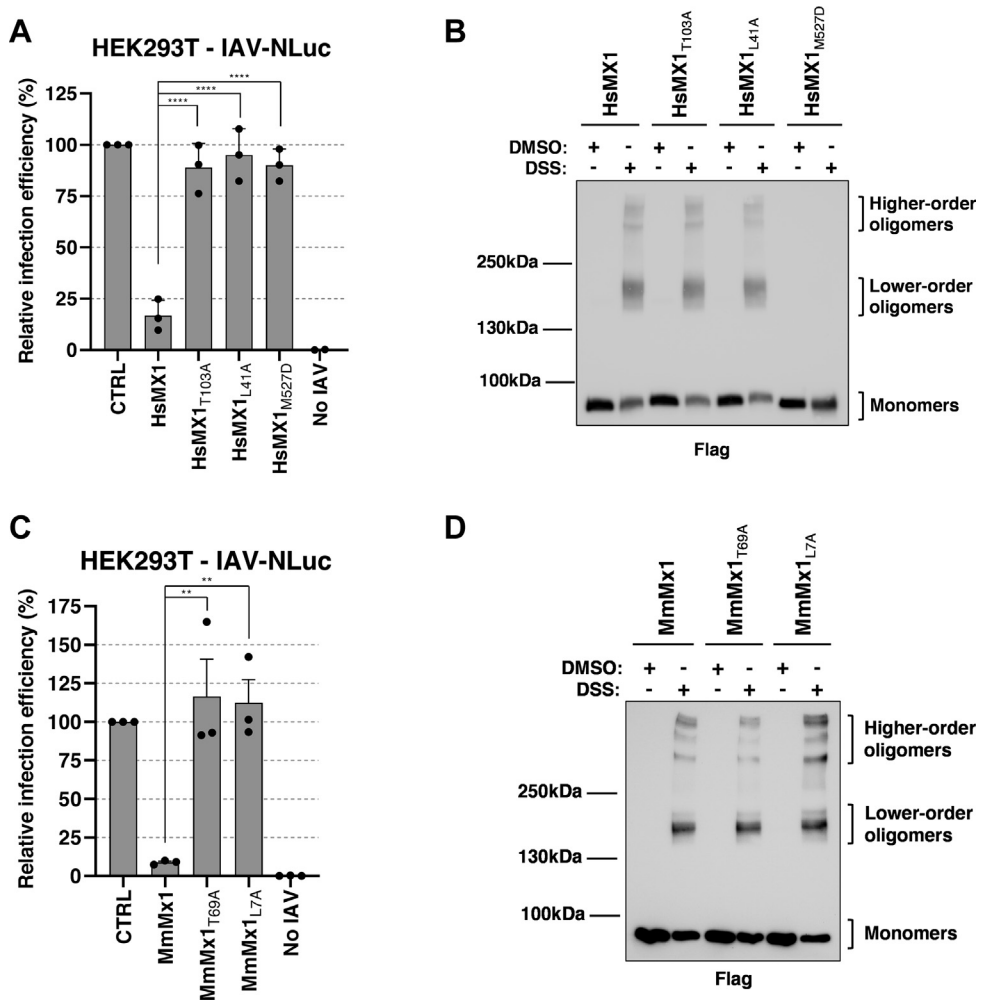

Figure 6. Chemical crosslinking indicates that the lack of antiviral activity of HsMX1$_{L41A}$ and MmMx1$_{L7A}$ is not due to an oligomerization defect. *A* and *C*, HEK293T cells were stably transduced to express FLAG-tagged HsMX1/MmMx1 proteins and mutants or E2-Crimson (CTRL), challenged with IAV-NLuc and relative infection efficiency was analyzed. The mean and SD of three independent experiments is shown. Ordinary one-way ANOVA multiple comparison with WT HsMX1 or MmMx1 was performed; ** = $p < 0.01$, **** = $p < 0.0001$. *B* and *D*, the same cells were lysed on ice, sonicated, and DSS (100 μg/ml) (or DMSO) treated for 60 min. After quenching, the lysates were resolved by SDS-PAGE and an immunoblot was performed to detect the FLAG-tagged MX1 proteins. Representative immunoblots are shown. DSS, disuccinimidyl suberate; DMSO, dimethyl sulfoxide; HEK293T, Human Embryonic Kidney 293T; IAV, influenza A virus.

33 to 60) were measured over time leading to very similar values for both angles between both WT and the L41A mutant (Fig. S3). Angle values were characteristic of α-helix structure with average values centered at −60° and −50° for Phi and Psi, respectively. This hinge or partial helix brake seems slightly more pronounced for WT HsMX1 than for the mutant when examining thoroughly angles values, however, this unique exception may not be sufficient to explain the difference observed in antiviral activity between the two proteins.

Therefore, this data suggests that the BSE domain extends slightly further than originally estimated, starting at S35, and that mutation of L41 into an alanine does not seem to impact BSE structural properties.

Discussion

Several HsMX1 intrinsic antiviral determinants have been described in the past, namely an active GTPase domain, the capability to oligomerize *via* the stalk, and intact BSE, L2, and L4 loops, but the importance of the N-terminal domain had never been assessed. In the case of HsMX2, the N-terminal domain was found to be one of the two main determinants, together with the oligomerization capacity, for anti-HIV activity (37, 38). Therefore, it was plausible that HsMX1 might also need this domain for antiviral activity despite a high variability between orthologous MX proteins (Fig. S1). Herein, we show that the N-terminal domain, more specifically the highly conserved leucine situated three amino acids before the (previously defined) start of the first BSE helix, from human, mouse, and bat (*S. lilium*) MX1 proteins, are essential for their anti-IAV activity. The importance of this leucine is highlighted by the fact that its mutation induces a complete loss of anti-IAV activity for all three proteins without being correlated with a decrease in protein expression levels or, for HsMX1 and MmMx1, without being correlated to a defect of oligomerization or of total inability to hydrolyze GTP. In addition, according to MD simulations based on the AlphaFold prediction, the mutation of L41 in HsMX1 into an alanine does not seem

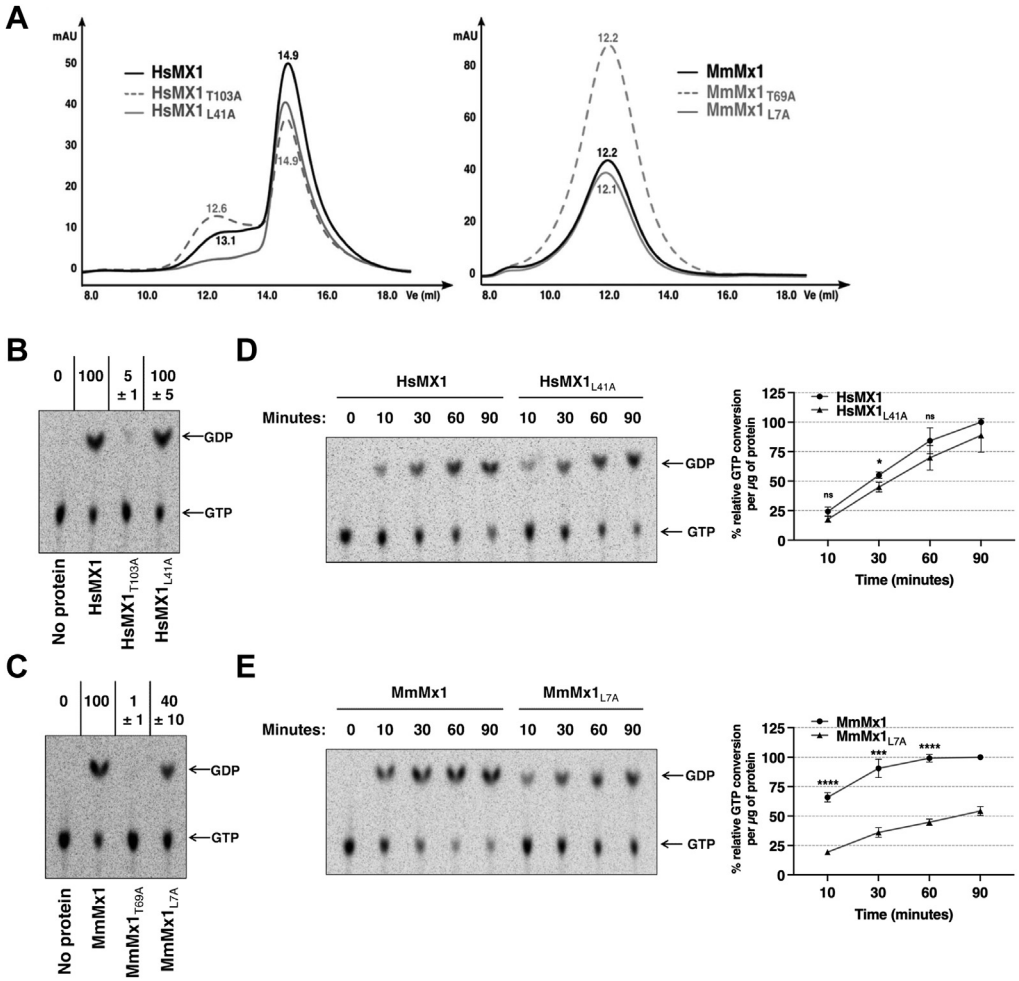

Figure 7. GTPase assays reveal that HsMX1$_{L41A}$ is catalytically active and that MmMx1$_{L7A}$ has a slightly impaired GTPase activity. *A*, recombinant WT and mutant FLAG-HsMX1 and FLAG-MmMx1 proteins were produced in *Escherichia coli* and purified. The elution profiles on Superose 6 increase 10/300 Gl column are shown for WT FLAG-HsMX1 and FLAG-MmMx1 proteins (*black lines*) in parallel to the indicated FLAG-tagged mutants (*gray continuous* and *dashed lines*). *B–E*, GTPase assays were performed with the recombinant proteins, and GDP and GTP levels were resolved using thin-layer chromatography (TLC) and visualized by autoradiography. *B*, representative TLC image for a 60-min GTPase assay with WT and mutant HsMX1 proteins. Numbers above the TLC represent the average of normalized signal intensity of the GDP spots from three independent experiments. *C*, similar to (*B*), with WT and mutant MmMx1 proteins and a 30-min GTPase assay. *D*, representative TLC image of a kinetic experiment performed on WT and L41 mutant HsMX1 (the GTPase assay was stopped at the indicated time points, *i.e.* 10, 30, 60, 90 min) (*Left*). The experiment was performed three times independently and the signals quantified and normalized to the 90-min time point for the WT protein (*Right*). *E*, Similar to (*C*), with WT and mutant MmMx1 proteins. *C* and *E*, *right panels*, the mean and SD of three independent experiments are shown. Paired Student *t* test was performed for the same time points between WT and mutant proteins; ns: nonsignificant, *$p < 0.05$, ***$p < 0.001$, ****$p < 0.0001$.

to affect the structure of the first BSE α-helix. Nevertheless, this residue was shown to be essential for subcellular localization of these three MX1 proteins. Finally, we show that this leucine is not only essential for HsMX1 restriction of IAV but also VSV, as well as LACV replication.

The N-terminal domain is not present in the crystal structure of HsMX1 (Fig. 1*A*), the nonstructured and highly flexible nature of this extension likely explains the lack of structural information (Figs. 1*A*, 8, *A*, and *B* and Movie S1). Furthermore, MmMx1 and SlMX1 3D structures have not yet been determined. As we now show that this conserved leucine is essential for the antiviral activity of these proteins, it would therefore be interesting to be able to decipher experimentally the structure of an MX1 protein with an intact N-terminal domain. This would allow us to understand the 3D architecture of this part of the protein and confirm the AlphaFold predictions. In terms of the role of this residue for MX1 function, we show above that it is not essential for the oligomerization of both HsMX1 and MmMx1 (Fig. 6, *B* and *D*). Of note, the elution profiles of the recombinant proteins are very similar for the WT and mutant proteins, confirming our crosslink data and the fact that the leucine point mutants do not seem to affect oligomerization status (Figs. 7*A*, 6, *B* and *D*). AlphaFold predictions nevertheless suggest that L41 is part of the α-helix of the first BSE (Fig. 8*A*), which, if confirmed experimentally, should lead to a redefinition of the boundaries of MX1 N-terminal and BSE domains. A plausible effect of these leucine mutants could therefore have been a partial hindrance to the correct folding or function of the first helix of the BSE, but MD simulations in this region for HsMX1 did not support this hypothesis as similar structural behavior was observed in both cases (Fig. 8, *B* and *C*, Movies S1 and S2). The AlphaFold prediction models

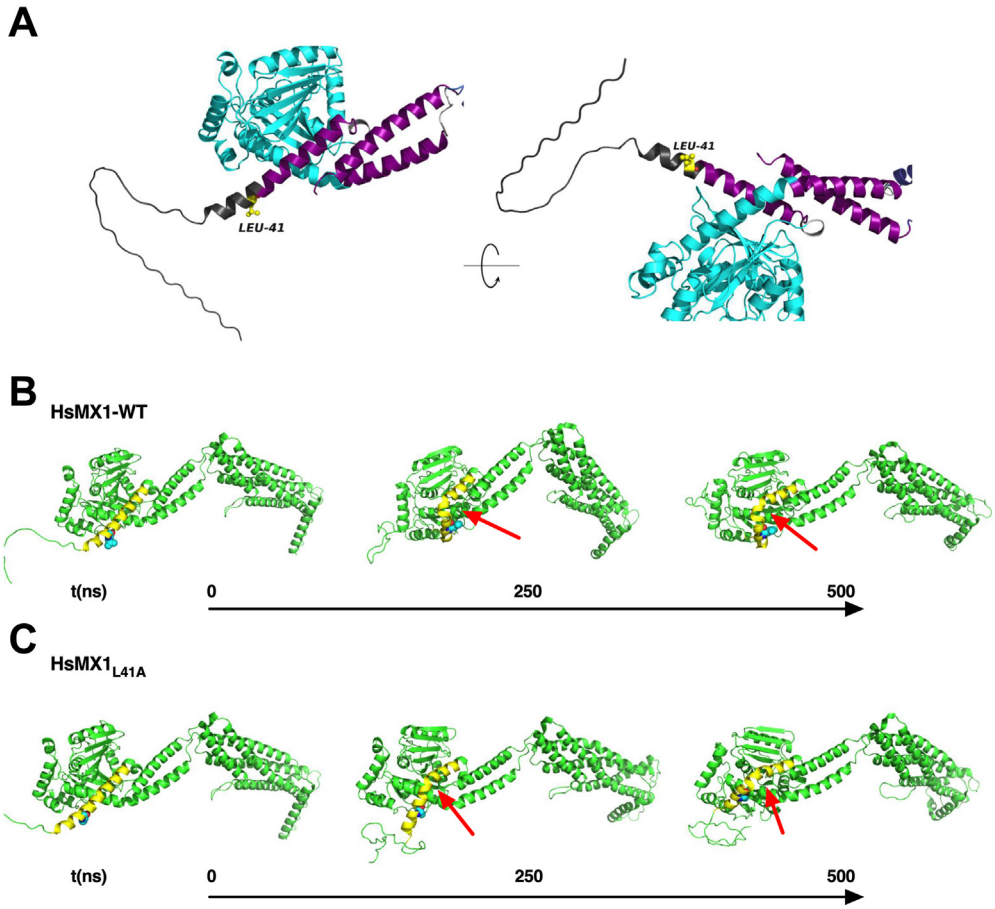

Figure 8. Mutation of L41 of HsMX1, which is predicted to be in an extended portion of the first BSE helix, does not affect BSE structural properties. *A*, Alphafold prediction of HsMX1-WT N-terminal domain with the position of L41 highlighted in *yellow*. BSE helices in *magenta*, G domain in *cyan*, and modelized N-terminal region in *black*. *B* and *C*, representative snapshots from MD simulations for WT HsMX1-WT (*B*) and $HsMX1_{L41A}$ (*C*) at three different time points (0, 250, and 500 ns). Full movies can be found in Movies S1 and S2. The N-terminal α-helix is highlighted in *yellow* and leucine 41 is depicted as *cyan spheres*. The secondary structure brake or turn occurring within this helix for both WT HsMX1 and $HsMX1_{L41A}$ is pointed by *red arrows*. BSE, bundle signaling element; MD, molecular dynamics.

the conserved leucine as pointing away from the core of the protein (Fig. 8, *A* and *B*). This could potentially suggest that L41 is a critical residue important for interaction with a cellular cofactor or a viral element, although the latter possibility is more difficult to imagine due to the wide breadth of viral families inhibited by MX1 proteins (7, 43). In support of the former idea, the subcellular localization of $HsMX1_{L41A}$, $MmMx1_{L7A}$, and $SlMX1_{L39A}$ were all displaced compared to their WT counterparts (Figs. 2*E*, 4, *B* and *D*). This might be explained by the loss of interaction with such a cellular cofactor, which would be essential for correct subcellular localization. This is further supported by the coexpression immunofluorescence experiments where in the presence of the WT protein, the mutant was able to correctly localize to the HsMX1 honeycomb-like network (Fig. S2*B*). The possibility of a loss of interaction with a critical cellular partner, when mutated at this residue, therefore seems a highly plausible possibility. Because of this, these single point leucine mutants present themselves as ideal candidates for differential interactomic approaches to identify such putative cellular cofactors. To date, no cofactor that would be essential for MX1 effector antiviral activity or correct subcellular localization has been identified. The discovery of such cofactor(s), if they exist, would probably be a major turning point to understand the mechanism of action of MX1 proteins.

Allelic variation studies have been performed for HsMX1 (50, 51), with only one variant being discovered in the N-terminal domain where a premature stop codon was found at amino acid position 30 (Q30*) causing a truncated, antivirally inactive protein (51). Using the gnomAD browser (https://gnomad.broadinstitute.org/), a single variant can be found in a single individual implicating L41 of HsMX1 where a missense deletion of one base occurred (21-42807777-AC-A) inducing a frameshift. With no reported naturally occurring allelic variation occurring at this position so far, it would be interesting to find such allelic variants to see if these individuals would be more susceptible to viral infections due to a non-functional HsMX1 protein.

The amino acid placed exactly three residues before the (previously defined) beginning of the first BSE α-helix is consistently a leucine for almost all studied species, with the exception of some fish species where it is replaced by a

phenylalanine (Fig. S1). We show that the only variation at this position that is accepted, among the residues tested, was that of leucine to phenylalanine (Fig. 5*B*), reinforcing the essential nature of the residue adopted at this position throughout evolution. Another interesting observation is the fact that when the N-terminal domain of HsMX2 was transferred onto HsMX1, this chimeric protein retained its anti-IAV activity while gaining anti-HIV activity (27). Despite being much longer than the N-terminal domain of HsMX1, HsMX2 also contains a leucine, three amino acids before the start of the BSE, which was therefore also the case for the chimeric protein (27). This information, coupled with the fact that the rest of the N-terminal domain is extremely divergent between species, attests to the high evolutionary selective pressure placed on this residue, further reinforcing the importance of this leucine (or in some cases, phenylalanine) for MX1 protein antiviral activity.

In conclusion, we show herein that the N-terminal domain of MX1 proteins, more specifically a highly conserved leucine residue, is important for their antiviral activity against multiple RNA viruses and governs correct subcellular localization. Further characterizing the importance of this residue could pave the way to a better understanding of the molecular mechanisms at play in the antiviral activity of these long-studied, yet still not well understood restriction factors.

Experimental procedures

Plasmid constructs

N-terminally FLAG-tagged HsMX1 and MmMx1 pCAGGS constructs were previously described (27). The N-terminally tagged Myc-HsMX1 was generated by PCR and inserted into a pCAGGS backbone. The *S. lilium* MX1-encoding plasmid was a gift from Prof Georg Kochs (44). All N-terminally FLAG-tagged HsMX1, MmMx1, and SlMX1 mutants were generated by overlapping PCR. Coding DNA sequences (CDSs) of interest were subcloned into pCAGGS using NotI and XhoI cloning sites. The pRRL.sin.cPPT.SFFV/IRES-puro.WPRE lentiviral vector (LV) system has been described previously (39). All LVs used here were obtained by subcloning of the CDSs of interest using NotI and either XhoI or SalI cloning sites. The pcDNA3-RFP-LACV-N construct was a gift from Prof Georg Kochs and generated by inserting the cDNA for mRFP1 (Addgene #14435) into pcDNA3 flanked by BamHI/NheI sites and then the LACV-N cDNA in frame with NheI/NotI. Bunyamwera N coding sequence (sequence ID: D00353.1) was synthetized (Eurofins) and cloned into pcDNA3-RFP in place of LACV-N, between NheI and NotI restriction sites, to generate pcDNA3-RFP-BUNV-N. pCAGGS-Renilla, pHSPOM1-Firefly, and pRRL.sin.cPPT.SFFV/FLAG-E2-Crimson-IRES-puro have previously been described (27).

The FLAG-HsMX1, FLAG-HsMX1$_{T103A}$, FLAG-HsMX1$_{L41A}$, FLAG-MmMx1, FLAG-MmMx1$_{T69A}$, and FLAG-MmMx1$_{L7A}$ CDS were PCR-amplified from the aforementioned pRRL.sin.cPPT.SFFV/IRES-puro.WPRE LV plasmids and cloned into pET-30 Ek/LIC expression vectors (Novagen) using KpnI and XhoI cloning sites. The different inserts are in frame with the S- and His-tags, and a sequence encoding the Tobacco Etch Virus protease cleavage site was inserted upstream of the FLAG-HsMX1, FLAG-MmMx1, and FLAG-mutant coding regions to enable tag removal during the protein purification process.

Cells, cell culture, transduction, and transfection

A549 (human lung adenocarcinoma; ATCC CCL-185), HEK293T (ATCC CRL-3216), Madin-Darby canine kidney (MDCK; ATCC CCL-34), African green monkey kidney (Vero; ATCC CCL-81), and Golden hamster kidney (BHK-21; ATCC CCL-10) cells were grown in Dulbecco's modified Eagle medium (DMEM) supplemented with 10% fetal bovine serum, 100 μg/ml penicillin and 100 units/ml streptomycin. Vero and BHK-21 cells were kind gifts from Dr Laurence Briant (IRIM). LV stocks were produced as described previously (39). Transduction with LVs was performed by incubating cells for 8 h prior to changing media for fresh media. Puromycin selection was performed 36 h post-transduction and cells were used for experiments once confluency was attained. Transfection experiments were performed using Lipofectamine 2000 (Thermo Fisher Scientific) according to the manufacturer's instructions.

Immunoblotting analysis

Cells were washed in PBS 1× and frozen dry at -80 °C or lysed directly in lysis buffer (10 mM Tris–HCl pH7.6, 150 mM NaCl, 1% Triton X100, 1 mM EDTA, 0.1% deoxycholate, 2% SDS, 5% glycerol, 100 mM DTT, 0.02% bromophenol blue) and boiled. The lysates were resolved by SDS-PAGE and analyzed by immunoblotting. Incubation with a primary FLAG antibody coupled to horseradish peroxidase (HRP) (mouse monoclonal M2, Sigma-Aldrich) and primary Myc coupled to HRP (Sigma-Aldrich) or Actin (Sigma-Aldrich) antibody followed by an HRP-conjugated secondary antibody was performed. Bioluminescence was then measured (Clarity ECL Western Blotting Substrate, Bio-Rad) using a ChemiDoc system (Bio-Rad).

Immunofluorescence and Airyscan confocal microscopy

A549 cells stably expressing the FLAG-tagged MX1 proteins or mutants of interest were plated into 24-well plates on coverslips at low density. The next day, cells were fixed using 2% paraformaldehyde in PBS 1× for 10 min at room temperature. Cells were permeabilized with 0.2% Triton X-100 in PBS 1× for 10 min followed by quenching and blocking in NGB buffer (50 mM NH_4Cl, 2% goat serum, 2% bovine serum albumin, in PBS 1×) for 1 h. Cells were incubated with primary antibodies (FLAG, Sigma-Aldrich, 1/1000, A5598; Myc, ProteinTech, 1/150, 16286-1-AP) for 1 h, washed, then incubated for 1 h with an Alexa Fluor–conjugated secondary antibody (Thermo Fisher Scientific). Cells were then incubated with Hoechst-33258 (Sigma-Aldrich) or DAPI (Thermo Fisher Scientific) for 5 min and mounted on glass slides using ProLong Gold Antifade Mountant (Thermo Fisher Scientific).

Almost all slides were imaged on an LSM880 confocal microscope with an Airyscan module (Zeiss) using a 63× objective. The coexpression experiments were acquired on an LSM980 Airyscan 8Y using a 63× objective. Processing of the raw Airyscan images was performed on the ZEN Black software. Postprocessing was performed using the FIJI software (52).

Quantification of RFP-LACV/BUNV-N HsMX1 aggregates

HEK293T cells were plated in 96-well plates and cotransfected with constructs of interest. Twenty four hours later, images of the transfected cells were acquired using an EVOS XL Core microscope (Thermo Fisher Scientific), and quantification of aggregated *versus* cytoplasmic RFP-LACV/BUNV-N phenotypes was performed manually on FIJI. Results were analyzed using GraphPad PRISM. For representative images, HEK293T cells were plated in 24-well plates on coverslips precoated with Poly-L-lysine (Sigma-Aldrich) and cotransfected with constructs of interest. Cells were fixed with 2% paraformaldehyde for 10 min, incubated with Hoechst-33258, and mounted as above, and images were acquired on an LSM880 confocal microscope with Airyscan module.

G-pseudotyped VSV*ΔG-fLuc particle production and infection

Luciferase-expressing G-pseudotyped VSV*ΔG-fLuc replicon particles were a gift from Dr Gert Zimmer (Institute of Virology and Immunology) and were produced as described in (41). 3×10^4 HEK293T cells were plated in 96-well plates and cotransfected with 0.04 μg of constructs of interest together with 0.015 μg of a Renilla luciferase-encoding pCAGGS plasmid (pCAGGS-Renilla). The following day, G-pseudotyped VSV*ΔG-fLuc replicon particle stock was diluted in complete DMEM and cells were infected at an MOI of 0.5. Sixteen hours post-infection, cells were frozen dry at −80 °C for 30 min and then lysed in Passive Lysis Buffer (Promega) for 30 min. Bioluminescence was measured using the Dual-Luciferase Reporter Assay System (Promega) on a microplate reader (Tecan Infinite Lumi). Firefly signals were normalized by Renilla luciferase levels and results were analyzed using GraphPad PRISM.

Virus production and infection

LACV was obtained from Prof Georg Kochs (Institut für Virologie) and amplified on BHK-21 cells in DMEM 2% fetal bovine serum, 20 mM Hepes. VSV (Indiana 1 serotype strain Mudd-Summers) was obtained from Dr Yves Gaudin (I2BC, Gif sur Yvette) and amplified on Vero cells in DMEM 10% serum. LACV and VSV viral stocks were titrated by plaque assays on Vero cells.

A/Victoria/3/75 (H3N2) containing the Nanoluciferase-coding sequence in the PA segment (IAV-NLuc reporter virus) was described before (39). A/Victoria/3/75 (H3N2) WT (IAV-WT) and IAV-NLuc were produced as described previously (8). Briefly, the eight Pol I plasmids (0.5 μg each) and four rescue plasmids (PB1, PB2, PA (0.32 μg each), and NP (0.64 μg)) were cotransfected into HEK293T cells in 6-well plates using Lipofectamine 3000 (Thermo Scientific). After 24 h, the cells were detached and cocultured with MDCK cells in 25 ml flasks. After 8 h of coculture in 10% serum, the medium was replaced with serum-free medium containing 0.5 μg/ml of TPCK-treated trypsin. Supernatants from day 5 post-transfection were used for virus amplification on MDCK cells. Viral stocks were titrated by plaque assays on MDCK cells. For IAV-NLuc reporter virus assays, A549 or HEK293T cells stably expressing the constructs of interest were infected at MOI 0.1 for 16 h. Levels of infection were measured as described above using the Nano-Glo Luciferase Assay System (Promega).

For the influenza minigenome infection reporter assay, 3×10^4 HEK293T cells were cotransfected in 96-well plates with 0.015 μg of pCAGGS-Renilla and 0.04 μg of pCAGGS-expressing FLAG-tagged MX1 mutants or controls and 0.03 μg of the minigenome plasmid pHSPOM1-Firefly. The negative sense, Firefly-coding minigenome transcribed from pHSPOM1-Firefly by the cellular RNA Pol I contains mutations 3-5-8 in the 3′ end of the promoter to increase replication and transcription efficiency following IAV infection (53). For the dominant-negative assay, HEK293T cells were transfected as above (0.03 μg of pHSPOM1-Firefly minigenome, 0.015 μg pCAGGS-Renilla, and 0.04 μg pCAGGS-expressing Myc-tagged HsMX1 or a control (pCAGGS-E2-Crimson)) together with an increasing amount (0.01, 0.02, 0.03, and 0.04 μg) of pCAGGS-expressing FLAG-tagged HsMX1-WT or mutants $HsMX1_{T103A}$ or $HsMX1_{L41A}$. Total amounts of DNA per transfection mix were adjusted with pCAGGS-E2-Crimson plasmid. Twenty four hours later, the cells were infected with WT A/Victoria/3/75 (H3N2) at MOI 0.1. Sixteen hours postinfection, cells were frozen dry at −80 °C for 30 min and lysed in Passive Lysis Buffer (Promega). Firefly and Renilla activities were then measured using the Dual-Luciferase Reporter Assay System (Promega). Firefly signals were normalized by Renilla luciferase levels. Results were analyzed using GraphPad PRISM.

Growth curve experiments

For IAV growth curve experiments, A549 cells stably expressing FLAG-tagged HsMX1, $HsMX1_{T103A}$, or $HsMX1_{L41A}$, seeded in 12-well plates, were infected in triplicate for 1 h at MOI 0.005 with A/Victoria/3/75 WT, washed with PBS, and incubated at 37 °C in 1 ml of serum-free DMEM containing 1 μg/ml of TPCK (Merck-Sigma). For VSV growth curve experiments and LACV infections, BHK-21 cells stably expressing FLAG-tagged HsMX1, $HsMX1_{T103A}$, or $HsMX1_{L41A}$, seeded in 12-well plates, were infected in triplicate for 2 h at MOI 0.005 (for LACV) or for 1 h at MOI 0.01 (for VSV) in DMEM without serum. Cells were then washed with PBS 1× and incubated at 37 °C in 1 ml of DMEM 2% serum, 20 mM Hepes (for LACV), or in 1 ml of DMEM 10% serum (for VSV). Samples were collected at different times post infection for viral titration by plaque assays on MDCK cells (for IAV) or on Vero cells (for LACV and VSV).

Cross-link experiments

Crosslinking experiments were performed as described in (54). Briefly, cells expressing the FLAG-tagged MX1 constructs of interest were lysed in 0.5% Triton X-100-PBS 1× buffer in the presence of complete protease inhibitor cocktail (Roche) for 20 min on ice. Lysates were water bath sonicated and centrifuged at 1500*g* for 10 min at 4 °C. Disuccinimidyl suberate (Thermo Fisher Scientific) was added at a final concentration of 100 μg/ml (or an equivalent volume of dimethyl sulfoxide was added to the control conditions) and incubated for 1 h at room temperature. Laemmli was added at 1× final and samples were resolved by SDS-PAGE without boiling on a 5% acrylamide gel. Immunoblotting was performed as mentioned above.

Protein expression and purification

The recombinant plasmids pET-30 Ek/LIC-expressing FLAG-HsMX1, FLAG-MmMx1, and FLAG-mutants were transformed in an *E. coli* BL21 (DE3) strain resistant to Phage T1 (New England Biolabs) carrying pRARE2. One colony was used to inoculate an overnight culture of 125 ml Lysogeny broth medium supplemented with kanamycin (50 μg/ml) and chloramphenicol (30 μg/ml). This culture was diluted in 2.5 l of Lysogeny broth medium supplemented with the two antibiotics. The cells were grown at 16 °C to an optical density at 600 nm of 0.8, then protein expression was induced with 1 mM IPTG and the culture was grown overnight at 16 °C. The cells were harvested by centrifugation at 8, 200*g* for 20 min and resuspended in 30 ml of buffer A (50 mM Tris–HCl pH 8, 400 mM NaCl, 5 mM $MgCl_2$, 7 mM β-mercaptoethanol, 40 mM imidazole, 10% glycerol, and 1 mM benzamidine). The cells were disrupted by sonication and cell debris were removed by centrifugation at 28, 000*g* for 60 min. The supernatant was loaded at 4 °C on Ni–NTA agarose beads previously equilibrated with buffer A. The beads were washed once with buffer A and twice with buffer B (50 mM Tris–HCl pH 8, 1 M NaCl, 5 mM $MgCl_2$, 7 mM β-mercaptoethanol, 40 mM imidazole, and 10% glycerol) and elution was performed with buffer E (50 mM Tris–HCl pH 8, 200 mM NaCl, 5 mM $MgCl_2$, 7 mM β-mercaptoethanol, 500 mM imidazole, 10% glycerol). The eluted protein was incubated with His-tagged Tobacco Etch Virus protease purified in our laboratory in a 1:100 (w:w) ratio; the cleavage reaction was performed during dialysis (dialysis-bag cutoff 12–15 kDa) against 1l dialysis buffer D (50 mM Tris–HCl pH 8, 200 mM NaCl, 5 mM $MgCl_2$, 5 mM β-mercaptoethanol) overnight at 4 °C. After dialysis, the proteins were centrifuged for 20 min at 28, 000*g* and the supernatant was loaded again at 4 °C on Ni–NTA agarose beads equilibrated with buffer D. The proteins without the His-tag were collected in the flow-through, concentrated to 5 mg/ml using a Vivaspin column (50 kDa cutoff, Sartorius), loaded onto a size-exclusion chromatography column (Superose 6 Increase 10/300 Gl, GE Healthcare), and eluted with buffer F (50 mM Tris–HCl pH 8, 500 mM NaCl, 5 mM $MgCl_2$, 0,5 mM β-mercaptoethanol, 10% glycerol). Aliquots of purified FLAG-tagged proteins were snap frozen in liquid nitrogen and stored at −80 °C.

GTPase activity assays

Recombinant FLAG-tagged, WT, and mutant HsMX1 or MmMx1 proteins (0.2 mg/ml) were incubated at 37 °C in GTPase assay buffer (50 mM Tris–HCl pH 8, 500 mM NaCl, 5 mM $MgCl_2$, 0,5 mM β-mercaptoethanol, 10% glycerol, 50 μM GTP, 26 nM [α-^{32}P]-GTP), as described previously (27). The reactions were stopped at the indicated time by addition of [2 mM EDTA, 0,5% SDS]. The reaction products were resolved by thin-layer chromatography (Merck Millipore) using thin-layer chromatography buffer (1 M LiCl, 1 M formic acid) and detected using phosphor screen autoradiography (Amersham Typhoon apparatus).

Molecular modeling and dynamic simulations of WT HsMX1 and $HsMX1_{L41A}$

HsMX1-WT (including the complete N-terminal domain and L4 loop) as well as $HsMX1_{L41A}$ were modeled using AlphaFold (48) through the ColabFold (55) platform. Predicted 3D models were compared to crystal (PDB: 3SZR) or low-resolution EM (PDB: 3ZYS) structures for examination of the overall folding of the three main domains (GTPase, BSE, and stalk) and also compared to 3D models based on these templates and built with Modeller v9.19 (56). Structural alignments of AlphaFold models and X-ray structure gave RMSD values (for all backbone atoms) of 0.4, 0.2, and 1.4 Å for GTPase, BSE, and Stalk domains, respectively. MD simulations were performed using NAMD3 (57) and CHARMM36m force field (58). Briefly, each protein was immersed in an explicit solvent box (TIP3P water model) using 10 Å of edge in each direction (in respect to protein dimensions), then neutralized with NaCl ions at a physiological concentration (0.154 M) and energy minimized for 50 ps using the conjugate gradients method. After a gradual heating from −273 °C to 37 °C, each system was further equilibrated for 300 ps using periodic boundary conditions to replicate the system in each direction. A trajectory of 500 ns was then produced (1 frame saved every 20 ps) for analysis in the isobaric-isothermal ensemble to keep constant temperature (37 °C) and pressure (1 atm) using Langevin dynamics and Langevin piston methods. The Newton's equation of motions was integrated using a timestep of 2 fs using the r-RESPA algorithm (59) with the short-range Lennard-Jones potential smoothly truncated from 10 to 12 Å and the PME (Particle Mesh Ewald) approach (60) used for calculating long-range electrostatics with a grid spacing of 1 Å. Trajectories analysis was performed using VMD (61), its Timeline plugin for per-residue Phi and Psi dihedral angles calculation, 3D-graphs (dihedral angles plots) were made with GnuPlot-5.4, and MD snapshots were illustrated with the PyMol Molecular Graphics System (v2.5, Schrödinger, LLC).

Statistical analyses

Statistical analyses were performed with the GraphPad Prism software. The analysis types performed are indicated in the figure legends. Comparisons are relative to the indicated condition. *p*-values are indicated as the following: ns = not significant, $p < 0.05$ = $^{*}p < 0.01$ = $^{**}p < 0.001$ = *** and $p < 0.0001$ = ****. No indication means the analyses were nonsignificant and were not represented for esthetic purposes.

Data availability

Datasets have been deposited on the public repository Science Data Bank (https://www.scidb.cn) and can be found using the following link: https://www.scidb.cn/s/JZFjia.

Supporting information—This article contains supporting information.

Acknowledgments—We are thankful to Prof Georg Kochs (Freiburg University, Germany) for the pcDNA3-RFP-LACV-N and SlMX1 plasmids as well as providing LACV; to Dr Gert Zimmer (Institute of Virology and Immunology, Switzerland) for the G-pseudotyped VSV*ΔG-fLuc luciferase particles; and to Dr Yves Gaudin (I2BC, Gif sur Yvette, France) for providing VSV. This work was supported by the institutional funds from the Centre National de la Recherche Scientifique (CNRS) and Montpellier University. We acknowledge the imaging facility MRI, member of the national infrastructure France-BioImaging supported by the French National Research Agency (ANR-10-INBS-04).

Author contributions—J. M., O. M., and C. G. conceptualization; J. M., M. A.-A., L. C., M. B., O. M., and C. G. methodology; J. M., M. A.-A., and M. B. validation; J. M., M. A.-A., and L. C. formal analysis; J. M., M. A.-A., L. C., M. T., C. A.-A., O. P., and O. M. investigation; J. M., O. M., and C. G. writing–original draft; J. M., M. A.-A., L. C., M. B., O. M., and C. G. writing–review and editing; J. M., M. A.-A., and L. C. visualization; L. C., M. B., and C. G. resources; M. B., O. M., and C. G. supervision; O. M. and C. G. project administration; C. G. funding acquisition; J. M., O. M., and C. G. data curation.

Funding and additional information—This work was supported by the European Research Council (ERC) under the European Union's Horizon 2020 research and innovation programme (grant agreement 759226, ANTIViR, to C. G.), the ATIP-Avenir program (to C. G.), the Institut National de la Santé et de la Recherche Médicale (INSERM) (to C. G.), a 3-year PhD studentship from the Ministry of Higher Education and Research (to J. M.) and a fourth year PhD funding from the Fondation pour la Recherche Médicale, grant number [FDT202106013175] (to J. M.), and institutional funds from IRIM (inter-team project, to M. A.-A. and M. B.). J. M., O. M., and C. G. acknowledge support from the French research network on influenza viruses (ResaFlu; GDR2073) financed by the CNRS.

Conflict of interests—The authors declare that they have no conflicts of interest with the contents of this article.

Abbreviations—The abbreviations used are: BSE, bundle signaling element; BUNV, Bunyamwera Virus; CDS, coding DNA sequence; DMEM, Dulbecco's modified Eagle's medium; HEK293T, Human Embryonic Kidney 293T; HRP, horseradish peroxidase; IAV, influenza A virus; IFN, interferon; LACV, La Crosse Virus; LV, lentiviral vector; MD, molecular dynamics; MDCK, Madin-Darby canine kidney; MOI, multiplicity of infection; RFP, red fluorescent protein; VSV, vesicular stomatitis virus.

References

1. Schoggins, J. W. (2019) Interferon-stimulated genes: what do they all do? *Annu. Rev. Virol.* **6**, 567–584
2. McKellar, J., Rebendenne, A., Wencker, M., Moncorgé, O., and Goujon, C. (2021) Mammalian and avian host cell influenza A restriction factors. *Viruses* **13**, 522
3. Lindenmann, J. (1962) Resistance of mice to mouse-adapted influenza A virus. *Virology* **16**, 203–204
4. Horisberger, M. A., Staeheli, P., and Haller, O. (1983) Interferon induces a unique protein in mouse cells bearing a gene for resistance to influenza virus. *Proc. Natl. Acad. Sci. U. S. A.* **80**, 1910–1914
5. Staeheli, P., Haller, O., Boll, W., Lindenmann, J., and Weissmann, C. (1986) Mx protein: constitutive expression in 3T3 cells transformed with cloned Mx cDNA confers selective resistance to influenza virus. *Cell* **44**, 147–158
6. Haller, O., Arnheiter, H., Pavlovic, J., and Staeheli, P. (2018) The discovery of the antiviral resistance gene Mx: a story of great ideas, great failures, and some success. *Annu. Rev. Virol.* **5**, 33–51
7. Haller, O., Staeheli, P., Schwemmle, M., and Kochs, G. (2015) Mx GTPases: dynamin-like antiviral machines of innate immunity. *Trends Microbiol.* **23**, 154–163
8. Goujon, C., Moncorgé, O., Bauby, H., Doyle, T., Ward, C. C., Schaller, T., *et al.* (2013) Human MX2 is an interferon-induced post-entry inhibitor of HIV-1 infection. *Nature* **502**, 559–562
9. Kane, M., Yadav, S. S., Bitzegeio, J., Kutluay, S. B., Zang, T., Wilson, S. J., *et al.* (2013) MX2 is an interferon-induced inhibitor of HIV-1 infection. *Nature* **502**, 563–566
10. Liu, Z., Pan, Q., Ding, S., Qian, J., Xu, F., Zhou, J., *et al.* (2013) The interferon-inducible MxB protein inhibits HIV-1 infection. *Cell Host Microbe* **14**, 398–410
11. Schilling, M., Bulli, L., Weigang, S., Graf, L., Naumann, S., Patzina, C., *et al.* (2018) Human MxB protein is a Pan-herpesvirus restriction factor. *J. Virol.* https://doi.org/10.1128/JVI.01056-18
12. Crameri, M., Bauer, M., Caduff, N., Walker, R., Steiner, F., Franzoso, F. D., *et al.* (2018) MxB is an interferon-induced restriction factor of human herpesviruses. *Nat. Commun.* **9**, 1980
13. Serrero, M. C., Girault, V., Weigang, S., Greco, T. M., Ramos Nascimento, A., Anderson, F., *et al.* (2022) The interferon-inducible GTPase MxB promotes capsid disassembly and genome release of herpesviruses. *Elife* **11**, e76804
14. Zimmermann, P., Mänz, B., Haller, O., Schwemmle, M., and Kochs, G. (2011) The viral nucleoprotein determines Mx sensitivity of influenza A viruses. *J. Virol.* **85**, 8133–8140
15. Engelhardt, O. G., Ullrich, E., Kochs, G., and Haller, O. (2001) Interferon-induced antiviral Mx1 GTPase is associated with components of the SUMO-1 system and promyelocytic leukemia protein nuclear bodies. *Exp. Cell Res.* **271**, 286–295
16. Engelhardt, O. G., Sirma, H., Pandolfi, P.-P., and Haller, O. (2004) Mx1 GTPase accumulates in distinct nuclear domains and inhibits influenza A virus in cells that lack promyelocytic leukaemia protein nuclear bodies. *J. Gen. Virol.* **85**, 2315–2326
17. Cao, Y.-L., Meng, S., Chen, Y., Feng, J.-X., Gu, D.-D., Yu, B., *et al.* (2017) MFN1 structures reveal nucleotide-triggered dimerization critical for mitochondrial fusion. *Nature* **542**, 372–376
18. Ramachandran, R., and Schmid, S. L. (2018) The dynamin superfamily. *Curr. Biol.* **28**, R411–R416
19. Gao, S., von der Malsburg, A., Paeschke, S., Behlke, J., Haller, O., Kochs, G., *et al.* (2010) Structural basis of oligomerization in the stalk region of dynamin-like MxA. *Nature* **465**, 502–506
20. Gao, S., von der Malsburg, A., Dick, A., Faelber, K., Schröder, G. F., Haller, O., *et al.* (2011) Structure of myxovirus resistance protein a reveals

intra- and intermolecular domain interactions required for the antiviral function. *Immunity* **35**, 514–525
21. Chen, Y., Zhang, L., Graf, L., Yu, B., Liu, Y., Kochs, G., *et al.* (2017) Conformational dynamics of dynamin-like MxA revealed by single-molecule FRET. *Nat. Commun.* **8**, 15744
22. Zheng, J., Cahill, S. M., Lemmon, M. A., Fushman, D., Schlessinger, J., and Cowburn, D. (1996) Identification of the binding site for acidic phospholipids on the pH domain of dynamin: implications for stimulation of GTPase activity. *J. Mol. Biol.* **255**, 14–21
23. Kochs, G., Haener, M., Aebi, U., and Haller, O. (2002) Self-assembly of human MxA GTPase into highly ordered dynamin-like oligomers. *J. Biol. Chem.* **277**, 14172–14176
24. Dick, A., Graf, L., Olal, D., von der Malsburg, A., Gao, S., Kochs, G., *et al.* (2015) Role of nucleotide binding and GTPase domain dimerization in dynamin-like myxovirus resistance protein A for GTPase activation and antiviral activity. *J. Biol. Chem.* **290**, 12779–12792
25. Zürcher, T., Pavlovic, J., and Staeheli, P. (1992) Nuclear localization of mouse Mx1 protein is necessary for inhibition of influenza virus. *J. Virol.* **66**, 5059–5066
26. Pitossi, F., Blank, A., Schröder, A., Schwarz, A., Hüssi, P., Schwemmle, M., *et al.* (1993) A functional GTP-binding motif is necessary for antiviral activity of Mx proteins. *J. Virol.* **67**, 6726–6732
27. Goujon, C., Moncorgé, O., Bauby, H., Doyle, T., Barclay, W. S., and Malim, M. H. (2014) Transfer of the amino-terminal nuclear envelope targeting domain of human MX2 converts MX1 into an HIV-1 resistance factor. *J. Virol.* **88**, 9017–9026
28. Yu, Z., Wang, Z., Chen, J., Li, H., Lin, Z., Zhang, F., *et al.* (2008) GTPase activity is not essential for the interferon-inducible MxA protein to inhibit the replication of hepatitis B virus. *Arch. Virol.* **153**, 1677–1684
29. Ponten, A., Sick, C., Weeber, M., Haller, O., and Kochs, G. (1997) Dominant-negative mutants of human MxA protein: domains in the carboxy-terminal moiety are important for oligomerization and antiviral activity. *J. Virol.* **71**, 2591–2599
30. Arnheiter, H., and Haller, O. (1988) Antiviral state against influenza virus neutralized by microinjection of antibodies to interferon-induced Mx proteins. *EMBO J.* **7**, 1315–1320
31. Flohr, F., Schneider-Schaulies, S., Haller, O., and Kochs, G. (1999) The central interactive region of human MxA GTPase is involved in GTPase activation and interaction with viral target structures. *FEBS Lett.* **463**, 24–28
32. Kochs, G., and Haller, O. (1999) Interferon-induced human MxA GTPase blocks nuclear import of Thogoto virus nucleocapsids. *Proc. Natl. Acad. Sci. U. S. A.* **96**, 2082–2086
33. Garber, E. A., Hreniuk, D. L., Scheidel, L. M., and van der Ploeg, L. H. (1993) Mutations in murine Mx1: effects on localization and antiviral activity. *Virology* **194**, 715–723
34. Patzina, C., Haller, O., and Kochs, G. (2014) Structural requirements for the antiviral activity of the human MxA protein against Thogoto and influenza A virus. *J. Biol. Chem.* **289**, 6020–6027
35. Verhelst, J., Spitaels, J., Nürnberger, C., De Vlieger, D., Ysenbaert, T., Staeheli, P., *et al.* (2015) Functional comparison of Mx1 from two different mouse species reveals the involvement of loop L4 in the antiviral activity against influenza A viruses. *J. Virol.* **89**, 10879–10890
36. Mitchell, P. S., Patzina, C., Emerman, M., Haller, O., Malik, H. S., and Kochs, G. (2012) Evolution-guided identification of antiviral specificity determinants in the broadly acting interferon-induced innate immunity factor MxA. *Cell Host Microbe* **12**, 598–604
37. Goujon, C., Greenbury, R. A., Papaioannou, S., Doyle, T., and Malim, M. H. (2015) A triple-arginine motif in the amino-terminal domain and oligomerization are required for HIV-1 inhibition by human MX2. *J. Virol.* **89**, 4676–4680
38. Busnadiego, I., Kane, M., Rihn, S. J., Preugschas, H. F., Hughes, J., Blanco-Melo, D., *et al.* (2014) Host and viral determinants of Mx2 antiretroviral activity. *J. Virol.* **88**, 7738–7752
39. Doyle, T., Moncorgé, O., Bonaventure, B., Pollpeter, D., Lussignol, M., Tauziet, M., *et al.* (2018) The interferon-inducible isoform of NCOA7 inhibits endosome-mediated viral entry. *Nat. Microbiol.* **3**, 1369–1376
40. Nigg, P. E., and Pavlovic, J. (2015) Oligomerization and GTP-binding requirements of MxA for viral target recognition and antiviral activity against influenza A virus. *J. Biol. Chem.* **290**, 29893–29906
41. Berger Rentsch, M., and Zimmer, G. (2011) A vesicular stomatitis virus replicon-based bioassay for the rapid and sensitive determination of multi-species type I interferon. *PLoS One* **6**, e25858
42. Kochs, G., Janzen, C., Hohenberg, H., and Haller, O. (2002) Antivirally active MxA protein sequesters La Crosse virus nucleocapsid protein into perinuclear complexes. *Proc. Natl. Acad. Sci. U. S. A.* **99**, 3153–3158
43. Verhelst, J., Hulpiau, P., and Saelens, X. (2013) Mx proteins: antiviral gatekeepers that restrain the uninvited. *Microbiol. Mol. Biol. Rev.* **77**, 551–566
44. Fuchs, J., Hölzer, M., Schilling, M., Patzina, C., Schoen, A., Hoenen, T., *et al.* (2017) Evolution and antiviral specificities of interferon-induced Mx proteins of bats against ebola, influenza, and other RNA viruses. *J. Virol.* https://doi.org/10.1128/JVI.00361-17
45. Schneider, T. D., and Stephens, R. M. (1990) Sequence logos: a new way to display consensus sequences. *Nucl. Acids Res.* **18**, 6097–6100
46. Crooks, G. E., Hon, G., Chandonia, J.-M., and Brenner, S. E. (2004) WebLogo: a sequence logo generator. *Genome Res.* **14**, 1188–1190
47. Janzen, C., Kochs, G., and Haller, O. (2000) A monomeric GTPase-negative MxA mutant with antiviral activity. *J. Virol.* **74**, 8202–8206
48. Jumper, J., Evans, R., Pritzel, A., Green, T., Figurnov, M., Ronneberger, O., *et al.* (2021) Highly accurate protein structure prediction with AlphaFold. *Nature* **596**, 583–589
49. Varadi, M., Anyango, S., Deshpande, M., Nair, S., Natassia, C., Yordanova, G., *et al.* (2022) AlphaFold protein structure database: massively expanding the structural coverage of protein-sequence space with high-accuracy models. *Nucl. Acids Res.* **50**, D439–D444
50. Graf, L., Dick, A., Sendker, F., Barth, E., Marz, M., Daumke, O., *et al.* (2018) Effects of allelic variations in the human myxovirus resistance protein A on its antiviral activity. *J. Biol. Chem.* **293**, 3056–3072
51. Chen, Y., Graf, L., Chen, T., Liao, Q., Bai, T., Petric, P. P., *et al.* (2021) Rare variant *MX1* alleles increase human susceptibility to zoonotic H7N9 influenza virus. *Science* **373**, 918–922
52. Schindelin, J., Arganda-Carreras, I., Frise, E., Kaynig, V., Longair, M., Pietzsch, T., *et al.* (2012) Fiji: an open-source platform for biological-image analysis. *Nat Met.* **9**, 676–682
53. Neumann, G., and Hobom, G. (1995) Mutational analysis of influenza virus promoter elements *in vivo*. *J. Gen. Virol.* **76**, 1709–1717
54. Dicks, M. D. J., Goujon, C., Pollpeter, D., Betancor, G., Apolonia, L., Bergeron, J. R. C., *et al.* (2016) Oligomerization requirements for MX2-mediated suppression of HIV-1 infection. *J. Virol.* **90**, 22–32
55. Mirdita, M., Schütze, K., Moriwaki, Y., Heo, L., Ovchinnikov, S., and Steinegger, M. (2021) ColabFold - making protein folding accessible to all. *Bioinformatics*. https://doi.org/10.1101/2021.08.15.456425
56. Šali, A., and Blundell, T. L. (1993) Comparative protein modelling by satisfaction of spatial restraints. *J. Mol. Biol.* **234**, 779–815
57. Phillips, J. C., Hardy, D. J., Maia, J. D. C., Stone, J. E., Ribeiro, J. V., Bernardi, R. C., *et al.* (2020) Scalable molecular dynamics on CPU and GPU architectures with NAMD. *J. Chem. Phys.* **153**, 044130
58. Huang, J., Rauscher, S., Nawrocki, G., Ran, T., Feig, M., de Groot, B. L., *et al.* (2017) CHARMM36m: an improved force field for folded and intrinsically disordered proteins. *Nat. Met.* **14**, 71–73
59. Tuckerman, M., Berne, B. J., and Martyna, G. J. (1992) Reversible multiple time scale molecular dynamics. *J. Chem. Phys.* **97**, 1990–2001
60. Essmann, U., Perera, L., Berkowitz, M. L., Darden, T., Lee, H., and Pedersen, L. G. (1995) A smooth particle mesh Ewald method. *J. Chem. Phys.* **103**, 8577–8593
61. Humphrey, W., Dalke, A., and Schulten, K. (1996) Vmd: visual molecular dynamics. *J. Mol. Graphics* **14**, 33–38